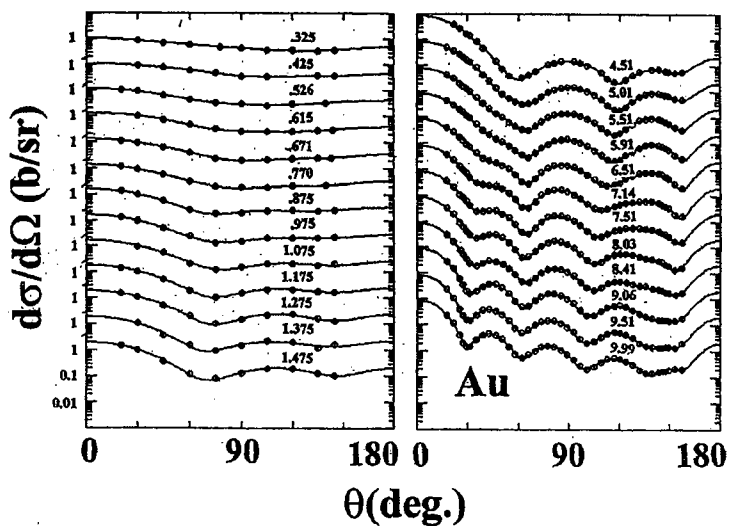


Neutron Scattering from the Standard ^{197}Au

Nuclear Data and Measurement Series

prepared by
Nuclear Engineering Division
Argonne National Laboratory



About Argonne National Laboratory

Argonne is managed by The University of Chicago for the U.S. Department of Energy under contract W-31-109-Eng-38. The Laboratory's main facility is outside Chicago, at 9700 South Cass Avenue, Argonne, Illinois 60439. For information about Argonne and its pioneering science and technology programs, see www.anl.gov.

Availability of This Report

This report is available, at no cost, at <http://www.osti.gov/bridge>. It is also available on paper to U.S. Department of Energy and its contractors, for a processing fee, from:

U.S. Department of Energy

Office of Scientific and Technical Information

P.O. Box 62

Oak Ridge, TN 37831-0062

phone (865) 576-8401

fax (865) 576-5728

reports@adonis.osti.gov

Disclaimer

This report was prepared as an account of work sponsored by an agency of the United States Government. Neither the United States Government nor any agency thereof, nor The University of Chicago, nor any of their employees or officers, makes any warranty, express or implied, or assumes any legal liability or responsibility for the accuracy, completeness, or usefulness of any information, apparatus, product, or process disclosed, or represents that its use would not infringe privately owned rights. Reference herein to any specific commercial product, process, or service by trade name, trademark, manufacturer, or otherwise, does not necessarily constitute or imply its endorsement, recommendation, or favoring by the United States Government or any agency thereof. The views and opinions of document authors expressed herein do not necessarily state or reflect those of the United States Government or any agency thereof, Argonne National Laboratory, or The University of Chicago.

Neutron Scattering from the Standard ^{197}Au

Nuclear Data and Measurement Series

by

Alan B. Smith

Nuclear Engineering Division, Argonne National Laboratory

The Physicist's Consultive, Ottawa, Illinois

June 2005

Keywords:

Measured neutron $d\sigma/\Omega_{el}$ for ^{197}Au , 4.5 \rightarrow 10.0 MeV.

Optical-statistical, coupled-channels, dispersion and "regional" models. Comparisons with ENDF/B-VL



THE UNIVERSITY OF
CHICAGO

Argonne National Laboratory is managed by
The University of Chicago for the U.S. Department of Energy

Table of Contents

Abstract	1
I. Introduction	1
II. Experimental Method	2
III. Experimental Results	3
IV. Physical Models	
IV-1. Spherical Optical-Statistical Model (SOM)	3
IV-2. Rotational Coupled-Channels Model (RCCM).....	5
IV-3. Dispersion Optical Models (DOM).....	6
V. "Regional" Models.....	8
VI. Comparisons with the ENDF/B-VI ¹⁹⁷ Au Evaluation	9
VII. Summary Remarks	10
Acknowledgements	12
References	12
Appendix A. ¹⁹⁷ Au neutron total cross section database	13
Appendix B. ¹⁹⁷ Au neutron elastic-scattering database	14
Appendix C. ¹⁹⁷ Au neutron inelastic-scattering database	15
Tables	17
Figures	24

Nuclear Data and Measurement Series

Reports in the Argonne National Laboratory Nuclear Data and Measurement Series present results of studies in the field of microscopic nuclear data. The primary objective of the series is the dissemination of information in the comprehensive form required for nuclear technology applications. This series is devoted to: a) measured microscopic nuclear parameters, b) experimental techniques and facilities employed in measurements, c) the analysis, correlation and interpretation of nuclear data, and d) the compilation and evaluation of nuclear data. Contributions to this Series are reviewed to assure technical competence and, unless otherwise stated, the contents can be formally referenced. THIS SERIES DOES NOT SUPPLANT FORMAL JOURNAL PUBLICATION, but it does provide the more extensive information required for technological applications (e.g., tabulated numerical data) in a timely manner.

Publications in the ANL/NDM Series

A listing of recent issues in this series is given below. Issues and/or titles prior to ANL/NDM-130 can be obtained from the National Technical Information Service, U. S. Department of Commerce, Technology Administration, Springfield, VA 22161, or by contacting the author of this report at the Nuclear Engineering Division, Argonne National Laboratory, 9700 South Cass Avenue, Argonne, IL 60439 (USA). In addition, the entire report series can be found on the Internet URL:-

<<http://www.td.anl.gov/reports/ANLNDMReports.html>>,

including abstracts, complete reports, and associated computer programs.

- A. B. Smith and P. T. Guenther
Fast-neutron interaction with the fission product ^{103}Rh
ANL/NDM-130, September 1993
- A. B. Smith and P. T. Guenther
Fast-neutron scattering from vibrational Palladium nuclei
ANL/NDM-131, October 1993
- A. B. Smith
Neutron interaction with doubly magic ^{40}Ca
ANL/NDM-132, November 1993
- A. B. Smith
Fast-neutron scattering at $Z=50$: - Tin
ANL/NDM-133, September 1994
- A. B. Smith, S. Chiba and J. W. Meadows
An evaluated neutronic data file for elemental Zirconium
ANL/NDM-134, September 1994

- A. B. Smith and S. Chiba
Neutron scattering from Uranium and Thorium
ANL/NDM-135, February 1995
- A. B. Smith
Neutron scattering and models: - Iron
ANL/NDM-136, August 1995
- A. B. Smith
Neutron scattering and models: - Silver
ANL/NDM-137, July 1996
- A. B. Smith and D. Schmidt
Neutron scattering and models: - Chromium
ANL/NDM-138, June 1996
- W. P. Poenitz and S. E. Aumeier
The simultaneous evaluation of the standards and other cross sections of
importance for technology
ANL/NDM-139, September 1997
- D. L. Smith and J. T. Daly
A compilation of information on the $^{31}\text{P}(p,\gamma)^{32}\text{S}$ reaction and properties of excited
levels in ^{32}S
ANL/NDM-140, November 2000
- A. B. Smith
Neutron scattering and models: - Titanium
ANL/NDM-141, July 1997
- A. B. Smith
Neutron scattering and models: - Molybdenum
ANL/NDM-142, July 1999
- R. E. Miller and D. L. Smith
Compilation of information on the $^{31}\text{P}(p,\gamma)^{33}\text{Cl}$ reaction and properties of excited
levels in ^{33}Cl
ANL/NDM-143, July 1997
- R. E. Miller and D. L. Smith
A compilation of information on the $^{31}\text{P}(p,\gamma)^{28}\text{Si}$ reaction and properties of the
excited levels in ^{28}Si
ANL/NDM-144, November 1997
- R. D. Lawson and A. B. Smith
ABAREX, a neutron spherical optical-statistical model code: - a user's manual
ANL/NDM-145, June 1999
- R. T. Klann and W. P. Poenitz
Non-destructive assay of EBR-II blanket elements using resonance transmission
analysis
ANL/NDM-146, 1998
- A. B. Smith
ELEMENTAL-ABAREX: - a user's manual
ANL/NDM-147, June 1999

- D. G. Naberejnev and D. L. Smith
A method to construct covariance files in ENDF/B formats for critical safety applications
ANL/NDM-148, June 1999
- A. B. Smith
Neutrons and antimony: - physical measurements and interpretations
ANL/NDM-149, July 2000
- A. B. Smith and A. Fessler
Neutrons and antimony: - neutronic evaluations of ^{121}Sb and ^{123}Sb
ANL/NDM-150, July 2000
- A. B. Smith
Fast neutrons incident on Holmium
ANL/NDM-151, December 2000
- R. D. Lawson and A. B. Smith
Technical note: - Dispersion contributions to neutron reactions
ANL/NDM-152, August 2001
- A. B. Smith
Fast-neutrons incident on Hafnium
ANL/NDM-153, June 2001
- D. L. Smith, Dimitri G. Naberejnev and L. A. Van Wormer
An approach for dealing with large errors
ANL/NDM-154, September 2001
- A. B. Smith
Fast-neutron scattering from elemental Rhenium
ANL/NDM-155, August 2003
- D. L. Smith
A demonstration of the lognormal distribution
ANL/NDM-156, July 2003
- A. B. Smith
Fast-neutrons incident on Gadolinium
ANL/NDM-157, April 2004
- D. L. Smith
A survey of experimental and evaluated fast-neutron Helium production data for fusion applications
ANL/NDM-158, May 2004
- D. L. Smith
Covariance matrices for nuclear cross sections derived from nuclear model calculations
ANL/NDM-159, January 2005
- A. B. Smith
Fast neutrons incident on rotors: - Tantalum
ANL/NDM-160, March 2005

ANL/NDM-161

NEUTRON SCATTERING FROM THE STANDARD ^{197}Au

by

Alan B. Smith ^{a,b}

^aNuclear Engineering Division, Argonne National Laboratory

^bThe Physicist's Consultive, Ottawa, IL

Abstract

Differential neutron "elastic scattering" cross sections of elemental gold are measured from $\approx 4.5 - 10.0$ MeV at incident-neutron energy intervals of ≈ 0.5 MeV. These results are combined with those of previous and lower-energy work by the author and associates to form a neutron-scattering database extending from $\approx 0.3 - 10.0$ MeV. This database is augmented with several additional scattering distributions and with detailed neutron total cross sections from the literature. The resulting composite database is interpreted in terms of optical-statistical, dispersion and coupled-channels models. The results are compared with relevant models in the literature, and a collective rotational model for the prediction of neutron interactions in this mass-energy region is proposed. The experimental and model results are compared with relevant portions of the ENDF/B-VI gold evaluated nuclear data file. Future work is suggested.

I. Introduction

Elemental gold is mono-isotopic (^{197}Au) and lies approximately midway between the region of heavy and highly deformed collective nuclei (e.g. the heavy fission products) and the spherical nuclei near the double shell closure at $Z = 82$ and $N = 126$. It is a transitional region between the strongly deformed rare earth nuclei and spherical ^{208}Pb over which there must be a qualitative change in nuclear shape and where the lower-energy excited structure of nuclei and their collective behavior is expected to change rather rapidly with mass. The gold isotopes in this region have been the subjects of extensive decay (NDS95) and stripping (Vie+78) studies which suggest that ^{197}Au is an asymmetric rotor as described by Davydov and Filippov (DF58) and by Hecht and Satchler (HS62). This model results in a number of rotational bands built upon the Mottelson and Nilsson (MN59, Pre62) collective-model orbital of the odd 79^{th} proton. The two lowest-energy of these are the $K=3/2^+$ [402] g.s. band, and the $K=1/2^+$ [400] band with its head at only 77 keV. These, and higher energy rotational bands, account for most, if not all, of the known states in ^{197}Au up to excitations of an MeV or more. Systematics indicate that the ^{197}Au deformation is oblate with the values of $\beta_2 = -0.131$ and $\beta_4 = -0.031$ (MNS95).

Over the last few years the author has given attention to the fast-neutron interaction with collective nuclei in the $A \approx 155 - 185$ highly-deformed region (Smi00, Smi01, Smi03, Smi04, Smi05). From these considerations has emerged a general "regional" behavior of the neutron interaction and a relevant model for interpolation and extrapolation, particularly to the prediction of neutron-interaction properties of the heavy fission products. The transition of this collective regional behavior in going to the spherical doubly closed shell is of both basic and applied interest. In the present context of ^{197}Au that transition may well be from symmetric rotors to asymmetric rotors and then to the spherical nuclei at the doubly closed shell. Fast neutron scattering is sensitive to low-energy target structure, as it is uninhibited by coulomb effects, and thus may be sensitive to the character of this transitional region. ^{197}Au is a heavy, non-corrosive metal, available in very high purities. It has electrical, chemical and mechanical properties that make it ideal for a number of special technical uses. Moreover, its neutron capture cross section is a primary standard over a wide incident-neutron energy range (ENDF/B-VI standards).

II. Experimental Method

The present measurements were made using the fast-neutron time-of-flight technique (CL55). The particular experimental apparatus and procedures have been extensively described elsewhere therefore only a brief outline will be given here (e.g. see SG92, Chi+92, But+82, Smi+67, and references cited therein). Ten ≈ 5 m. long flight paths were concurrently used. They were variable in neutron scattering angle over the range of $\approx 20 - 165$ deg. The neutron source was the $\text{D}(d, n)^3\text{He}$ reaction (Dro87) with the deuterium target gas contained in a 2.5 cm. long cell at a pressure of two atmospheres. The scattering sample was a 2-cm. diameter and 2-cm. long cylinder of high-purity elemental gold placed ≈ 14 cm. from the neutron source at a zero-degree source-reaction angle. The neutron source was pulsed at a repetition rate of 1 MHz with a burst duration of ≈ 1 nsec. The scattered-neutron detectors were ≈ 12.5 cm. diameter and ≈ 2 cm. thick hydrogenous scintillators employing pulse-shape discrimination to suppress gamma-ray detection. The source intensity was monitored with ancillary time-of-flight detectors. The relative energy-dependent responses of the scattered-neutron detectors were established by observing the energy spectrum of neutrons emitted at the spontaneous fission of ^{252}Cf (SGS77), and the absolute normalizations were determined by observation of neutrons scattered in the well-known standard reaction $\text{H}(n, n)$ (CSL83). The relative neutron scattering angles were optically determined to 0.1 deg. and the angular scale normalized by the observation of neutron scattering from polyethylene either side of the apparent centerline. All the results were corrected for angular resolution, beam attenuation and multiple-event effects using Monte-Carlo techniques (Smi91). The earlier and lower-energy work reported by the author and co-workers (deV+65) used essentially the same experimental methods, but with shorter (≈ 2 m) flight paths and smaller neutron detectors whose response was normalized to neutron scattering from elemental carbon (Lan+61).

III. Experimental Results

The present experimental results consist of twelve "elastic"-scattering distributions approximately equally spaced in incident energy between $\approx 4.5 - 10.0$ MeV. The scattered-neutron experimental resolutions were ≈ 0.3 MeV, so these "elastic" distributions certainly included inelastically-scattered contributions due to the excitations of the 77 keV (1/2+), 269 keV (3/2+) and 279 keV (5/2+) states in ^{197}Au . These angular distributions generally consisted of ≈ 40 or more differential values distributed between $\approx 20 - 160$ deg. Experimental uncertainties, including systematic and statistical contributions, are $\approx 3 - 5\%$, except near the minima of the distributions where they are larger. These experimental results are shown in Fig. 1, together with the prior lower-energy work by the author and his associates (deV+65). They very largely dominate the knowledge of fast-neutron "elastic" scattering from ^{197}Au , as outlined in Appendix B. There is very little else known; nothing between $\approx 1.5 - 4.5$ MeV nor above ≈ 15.0 MeV.

IV. Physical Models

IV-1. Spherical Optical-Statistical Model (SOM)

^{197}Au , with an asymmetry $((N-Z)/A) = 0.198$, lies between the $A \approx 150 - 180$ region of large collective deformations and the spherical region of the doubly closed shells ($Z = 82$ and $N = 126$) at ^{208}Pb . Thus the interaction of fast neutrons with pseudo-spherical ^{197}Au should be reasonably approximated with a conventional spherical optical-statistical model (Fes58, Hod63, FPW54, Wol51). Such a model can serve to meet many fundamental and applied needs and it is a basis for more detailed considerations of collective effects, e.g. via coupled-channels analysis (see Section IV-2, below) or DWBA calculations. The present SOM considerations have the objective of meeting some of these basic and applied needs, and of providing a comparative test of other global and regional spherical optical models suggested in the literature (e.g. KD03).

Throughout this work the real potential was assumed to have the Saxon-Woods form, and the imaginary potential the surface Saxon-Woods Derivative form. A real spin-orbit potential of the Thomas form was used with the parameters of Walter and Guss (WG85). These potential forms are defined by Hodgson (Hod63), and many others. There was no imaginary spin-orbit potential. The available differential neutron-scattering experimental data extends only to 14.6 MeV so the present model considerations are directed toward incident energies below 15 MeV and thus are not sensitive to volume absorption. The neutron excitation of the ground and the first twelve excited states of ^{197}Au were explicitly considered using the energies, spins and parities given in the Nuclear Data Sheets (NDS95). All of the neutron interactions with these states consisted of compound-nucleus processes in the context of the SOM, and their treatment included resonance width fluctuation and correlation corrections in the manner of Moldauer (Mol80). Higher-energy excitations were considered using the statistical continuum model and parameters of Gilbert and Cameron (GC65). Neutron capture is small at the energies of the present measurements and thus was not considered in the

SOM potential derivations, though the final SOM was used to estimate some of the capture and inelastic neutron-scattering processes. Other neutron-induced reactions were ignored, as they are generally small at the energies of the present considerations. Most of the spherical model calculations were carried out with the code ABAREX (LS99), with some additional spherical calculations using versions of the code ECIS96 (Ray95). In a spherical context these two codes gave essentially identical results. All of the fitting calculations gave careful attention to the experimental resolution of the measured data, combining calculated elastic and inelastic scattering contributions where warranted to be consistent with experimental resolutions.

The derivation of the SOM parameters was based entirely upon measured neutron differential “elastic” scattering and neutron total cross sections at energies concurrent with those of the “elastic” scattering distributions. There are experimental neutron total cross sections to more than 500 MeV but no angle-differential scattering results above ≈ 14.6 MeV (see **Appendices A and B**). The total cross sections used in the potential derivations were interpolated from the energy-averaged values defined in **Appendix A** and illustrated in **Fig. A-1**. They were exactly energy correlated with those of the experimental differential “scattering” values. At lower energies (below 1.5 MeV) the latter were constructed from the lower-energy “elastic” scattering distributions reported some time ago by the author and co-workers (deV+65), augmented with some additional unpublished results from the author’s files. These lower-energy scattering data consisted of many distributions, which were averaged over approximately 100 keV incident-energy intervals using legendre-polynomial expansions to interpolate in angle. All of these “elastic” distributions fully resolved the elastic component from inelastic contaminations up to ≈ 1.0 MeV. At incident energies of 1.0 to 1.5 MeV many of them included contributions from the inelastic neutron excitation of the first 77 keV level in ^{197}Au . These lower-energy averaged distributions are illustrated in the left panel of **Fig. 1**. The higher energy “elastic” distributions used in the model derivations were largely taken directly from the present measurements. There are twelve of these approximately equally spaced in energy between 4.5 and 10.0 MeV. Each of the latter contained inelastically scattered contributions due the excitation of ^{197}Au levels up to approximate 300 keV. These higher-energy contributions are illustrated in the right panel of **Fig. 1**. To this differential scattering database were added several selected distributions from the literature (see **Appendix B**), particularly the 14.6 MeV distribution of Hansen et al. (Han+85). The resulting 31 “elastic” distributions used in the model derivations are illustrated in **Fig. 2**, for example. They span the $\approx 0.3 - 15.0$ MeV energy range with nothing in the $\approx 1.5 - 4.5$ interval or above 15.0 MeV. The uncertainties of the individual differential values were accepted as given by the respective authors or, when necessary, as estimated by the present author.

The SOM parameters were obtained by least-square fitting the above neutron total cross section and “elastic”-scattering database. The fitting followed the six sequential steps long used by the author: - i) first determining the real potential diffuseness (a_V), ii) the real-potential reduced radius (r_V) (where $R_i = r_i \cdot A^{1/3}$), iii) the imaginary reduced radius (r_W), iv) the imaginary diffuseness (a_W), v) the real depth (V), and finally vi) the imaginary depth (W). The uncertainties utilized in the fitting of the

scattering values were as noted above, and the weight of the corresponding total cross sections was generally set to be equivalent to that of 15 differential scattering values, although other total-cross-section weights were examined ranging from 0.0 (ignore total cross sections) to the equivalent of 50 differential values. The resulting spherical potential parameters are given in Table 1. These parameters describe the differential scattering data as illustrated in Fig. 2. While the scattering data below 1.5 MeV is reasonably described, it lacks the "character" that is sensitive to model parameters. The data from 4.5 to 15 MeV is also reasonably described but for the defraction minima where the calculated results can be much smaller than the measured values. This is not surprising as it is in just such regions where the impact of collective effects will be largest, and ^{197}Au is a collective rotator (see following section). The potential of Table 1 also gives a qualitatively reasonable description of the observed neutron total cross sections, as illustrated in Fig. 3. Throughout the energy range of the data used in the model derivation, and thus the region of primary model applicability, the calculated and measured total cross sections generally agree within the total-cross-section experimental uncertainties alone, except at the very lowest energies. That is a region where the total cross section database may be distorted by self-shielding and where the measurement sets are not very consistent. The SOM of Table 1 results in a S_0 strength function of 2.329 and a S_1 strength function of 0.540 (in units of 10^{-4}) compared with the values 2.0 ± 0.1 and 0.4 ± 0.1 , respectively, deduced from resonance measurements (MDH81). At higher energies the calculated total cross sections tend to become a little too large. However, generally the potential of Table 1 seems to be a reasonable spherical parameterization of the fast-neutron interaction with ^{197}Au at incident energies up to at least 20 MeV.

IV-2. Rotational Coupled-Channels Model (RCCM)

The RCCM approximates the ^{197}Au asymmetric rotor with a spherical rotor coupling the g.s., $(3/2^+)$, 0.279 keV $(5/2^+)$ and 0.548 keV $(7/2^+)$ levels of the $K = 3/2^+[402]$ first rotational band. The remaining excited levels, including those of the $K = 1/2^+[400]$ band, were treated as straight-forward compound-nucleus excitations up to excitation energies of 1.1 MeV. Higher-energy excitations were also taken to be compound-nucleus processes using the statistical model and parameters of Gilbert and Cameron (GC65), as in the above SOM. Where appropriate, all compound-nucleus calculations again included resonance correlation and fluctuation corrections in the manner of Moldauer (Mol80).

The RCCM fitting procedures were similar to those used in the SOM derivations (above) with the addition of the rotational coupling. The parameter selection was based entirely upon least-square fitting of the same "elastic" distributions used in the above SOM context. Neutron total cross sections were not a part of the fitting procedure but were compared with the calculated results at each step to guide the fitting. The RCCM fitting followed two regimes. The first was analogous to the six-parameter fitting of the above SOM derivation. The second accepted the "regional" geometric parameters of Smith (Smi05) and the fitting was limited to the two parameters, real and imaginary potential depths. Again, the spin-orbit potential was taken from Walter and Guss

(WG85) and the continuum of compound-nucleus excitations from the statistical model and parameters of Gilbert and Cameron (GC65). The large majority of the RCCM calculations assumed that the β_2 and β_4 deformations were negative, i.e. represented oblate deformations. This is consistent with the compilation of Moeller, Nix and Swiatecki (MNS95). Some of the better potentials were subsequently used to repeat the calculations using various positive β values, i.e. implying prolate deformations. The differences between calculated results using oblate or prolate assumptions were quite small, smaller than can be reasonably distinguished from the available neutron data in the present considerations. The results of a large number of choices of β_2 between -0.05 and -0.30 , and of β_4 between -0.01 and -0.04 were examined. The calculated results are reasonably sensitive to the β_2 values. The fitting suggests that β_2 is in the range -0.10 to -0.15 and β_4 is ≈ -0.03 . These values are qualitatively consistent with systematic behavior (MNS95), and indicate a far more spherical nucleus than the highly deformed targets in the range $A \approx 152 \rightarrow 187$ (Smi05). The available neutron data is not precise enough to provide more accurate definitions of the β s. The RCCM parameters resulting from the six-parameter fitting are given in Table 2 and those obtained from the two parameter fitting in Table 3. The measured neutron total cross sections and those calculated with the RCCM potentials of Tables 2 and 3 are compared in Fig. 4. Both RCCM potentials give good descriptions of the observed total cross sections, with that of Table 3 slightly the superior. In both examples, the difference between measurement and calculation is approximately equivalent to the experimental uncertainty alone. The measured differential "elastic" scattering calculated with the two RCCM potentials is also very similar (compare Figs. 5 and 6) and both are reasonably descriptive of the measured differential cross sections. The largest differences between measured and calculated differential values is near the first minimum of the first few distributions above incident energies of ≈ 4.5 MeV. This is an angle-energy region that may be sensitive to the details of the collective structure and therefore to asymmetric rotational properties not dealt with in the spherical rotational model assumed for the RCCM.

The geometry resulting from the 6-parameter fitting is quiet different from that of the "regional" potential used in the 2-parameter fitting (compare Tables 2 and 3). In particular, the 6-parameter fitting leads to an imaginary radius that is much larger than the real radius, and to a much reduced imaginary-potential diffuseness. The latter geometric trends also are characteristic of the SOM values of Table 1. However, the real and imaginary potential strengths of Tables 2 and 3, in volume-integrals-per-nucleon, differ by only a very few percent.

IV-3. Dispersion Optical Models (DOM)

In order for the optical potential to be an analytical function, its real and imaginary parts are interconnected by a dispersion relation (JLM77, Lan62, Sat83, Lip66, Pas57 and Fes58). This interrelation can be expressed in the integral form

$$J_V(E) = J_{HF}(E) + (P/\pi) \cdot \int [J_W(E') / (E-E')] \cdot dE' \quad (1)$$

where J_V is the strength of the real potential, J_{HF} that of the local equivalent Hartree-Fock potential, and J_W the strength of the imaginary potential (throughout this section potential strengths are given as volume-integrals-per-nucleon unless otherwise stated). P denotes the principle value of the integral, which is evaluated from $-\infty$ to $+\infty$. Of course, the problem is that the potentials are not known from $+$ to $-\infty$ and some rather qualitative approximations must be made to evaluate the above integral. In the present application it was assumed that the surface imaginary potential rises linearly with energy from the zero-energy value to a 15 MeV value and then falls linearly to zero magnitude at 80 MeV. Concurrently a volume imaginary potential is assumed to rise linearly with energy from a zero value at 15 MeV to the 15 MeV strength of the surface imaginary at 80 MeV, and then remains constant with energy on to infinity. This behavior is here termed "DISP-A". Alternatively, the 80 MeV volume-imaginary potential strength is taken to be only 1/10 that of the 15 MeV surface value. This latter behavior is here termed "DISP-B". These are two quite different extrapolations of the high-energy behavior of the imaginary potential and they lead to different dispersion results. It was assumed that the surface imaginary potential rises quadratically from zero at the fermi energy to the zero energy value, and it was further assumed that the entire imaginary potential was symmetric about the fermi energy, taken to be -7.29 MeV as determined from the Nuclear Wallet Cards (Tul90). These "DISP-A" and "DISP-B" assumptions of higher-energy behavior are relative extreme cases. Other alternative assumptions are, of course possible. Also, the relative geometric shapes of both surface and volume imaginary potentials may be energy dependent, not fixed as assumed here. There are similar integrals of the volume aspects of the imaginary potential but they will be largely absorbed in the energy dependence of the real potential and thus are not defined by experiment. They will, however, impact on the energy dependence of the real potential and thus on the apparent effect of the non-locality of the nuclear force on the real potential, a matter that has received little attention in the literature. These dispersion concepts, the associated integrals, and the mathematical methods for their evaluation are discussed in detail by Lawson, Guenther and Smith (LGS87) and by Lawson and Smith (LS01). The definitions and methods of these two references were used to evaluate the J_V of Eq. 1 in the context of the SOM whose potential is given in Table 1. The calculations based upon the above two assumptions of the high energy imaginary-potential behavior determine the fraction of the surface potentials added to the real potential as a function of energy as illustrated in Fig. 7. This fraction (DISP-A and DISP-B of the figures) falls from near unity at zero energy to small positive and/or negative values at the upper energies of the present experimental database depending upon the assumed high-energy extrapolation of the imaginary potential. These dispersion-fraction energy dependencies are expressed as cubic energy expansions in the present calculations, as given in Tables 4 and 5. The experimental database was refitted assuming either these two DISP effects using six parameter fitting analogous to the derivation of the above SOM. This fitting in each "DISP" case proceeded in three iterative cycles for each of the dispersion assumptions. The resulting spherical dispersion-model parameters are given in Tables 4 and 5. Both of the DISP assumptions led to potentials that are similar as evident from comparisons of these two Tables. They both resulted in arguably improved descriptions of the ^{197}Au neutron total cross sections compared to those obtained with above SOM alone, as illustrated in Fig. 8. The differential "elastic" distributions were also very

similar to those obtained with the simple SOM as illustrated by comparing Fig. 2 and Fig. 9. The potential strengths and geometries of the two dispersion potentials are different from each other and from those of the SOM. In particular, the energy dependence of the real potential differs in all three cases. This effect will impact upon considerations of the non-locality of the nuclear force. These dispersion potentials also have smaller real radii than the SOM. This is a reasonable implication of the introduction of a surface component into the real potential as a result of the dispersion. These variants suggest that it will be difficult to experimentally distinguish dispersion from non-locality effects, or from any other effect that leads to energy-dependent variations in potential shapes, without careful attention to dispersion effects.

V. "Regional" Models

Over the last several years the author has considered the fast-neutron interaction with heavy, rare-earth, collective vibration and rotational nuclei. These targets are in the mass interval $A \approx 152 - 186$, have prolate deformations in the range $\beta_2 \approx 0.160$ to 0.300 , and asymmetries of ≈ 0.170 to 0.195 . The results are described in references Smi00, Smi01, Smi03, Smi04 and Smi05, and also in the Los Alamos results of references MY87 and YA87. The real and imaginary potential strengths (expressed as volume-integral-per-nucleon) are remarkably similar, as summarized in Table 6A. From their average the "regional" potential strength is quite well determined as given in Table 6A. There is more scatter in the geometric parameters, but the "regional" averages in Table 6B are very successful in the geometric description of, not only the highly deformed collective targets of Table 6A, but also in the present study of the less collectively deformed ^{197}Au , as described in Section IV-2, above. The averaged potential strengths and geometries of Tables 6A and 6B are very descriptive of the fast neutron interaction with the heavy and collectively deformed nuclei up to incident neutron energies of at least 20 MeV. For ^{197}Au the regional geometries remain suitable but the real and imaginary potential strengths are markedly less as noted in Table 6A, and in Section IV-2. In this transitional region one can hope that the regional geometry continues to retain its validity, with the structural changes reflected in decreasing potential strengths as the doubly-closed shell at ^{208}Pb is approached. The effect is illustrated in Fig. 10 where neutron total cross sections of ^{197}Au , as calculated with the regional potential of Table 6A and 6B, are compared with those determined with the potential of Table 3. The "regional" potential strengths clearly are not appropriate for ^{197}Au , while the "regional" potential geometries remain reasonably valid. The same conclusion was reached when measured and calculated differential elastic distributions were compared. It will be interesting to extend these comparisons to the double shell closure.

Additional comparisons of measured (symbols) and calculated (curves) neutron total neutron cross sections of ^{197}Au are shown in Fig. 11. Panel A of that figure shows the results calculated with the general spherical optical model of Koenig and Delaroche (KD03) (ignoring volume absorption at these low energies of < 20 MeV, and using statistical continuum parameters of reference GC65). Panel B shows similar comparisons obtained with the present spherical potential of Table 1. ^{197}Au is nearly spherical so both

of these SOMs do reasonably well though they tend toward a bit too large results at 20 MeV. Panel C illustrates the results obtained using the ^{181}Ta rotational potential of Smith (Smi05), only with the deformations lowered to the smaller ^{197}Au values of $\beta_2 = -0.100$ and $\beta_4 = -0.031$. The result is qualitatively acceptable agreement but, again, calculated values tend to become too large as 20 MeV is approached. For comparison, Panel D of Fig. 11 illustrates the results obtained with the present RCCM of Table 3. The latter model is clearly the more desirable.

VI. Comparisons with the ENDF/B-VI ^{197}Au Evaluation

The knowledge of the fast-neutron total cross sections of ^{197}Au is summarized in Appendix A. This information was energy averaged, as described in that Appendix, with the results illustrated in Fig. A-1. These energy-averaged ^{197}Au total cross sections are in remarkable agreement with the values given in ENDF/B-VI, as illustrated in Fig. 12. It is noted that the evaluation and one of the major experimental data sets ((Abf01) of Appendix A) came from the same institution. Fig. 12 also shows the results calculated with the RCCM and potential of Table 3. Again, the agreement is excellent except possibly for the very lowest energies.

The evaluated neutron angle-integrated elastic-scattering cross sections of ^{197}Au are compared with those calculated with the present RCCM of Table 3 in Fig. 13. Above ≈ 7 MeV the agreement between the evaluation and the calculation is remarkably good. At lower incident energies the ENDF/B-VI elastic scattering falls increasingly below the results based upon the present work as the energy decreases. The discrepancy becomes $\approx 10\%$ at few-MeV energies, and will impact upon other evaluated partial cross sections, as the evaluated file must be internally consistent. That impact will probably be greatest on the partial inelastic neutron-scattering cross sections. The same sort of discrepancies are evident in comparisons of differential elastic-scattering angular distributions, as illustrated in panels A, B, C and D of Fig. 14. Again, the agreement between the evaluation and the results of the present work is remarkably good above ≈ 7 MeV but deteriorates as the incident energy decreases.

The fast-neutron capture cross section of ^{197}Au is a recommended neutron-capture reference standard (ENDF/B-VI) due to its size, precision and ease of experimental usage. The present work is relevant to that standard cross section. The potential of Table 1 was used to calculate it following the methods of Lawson and Smith (LS99). The necessary binding energies were taken from Wapstra, Audi and Hoekstra (WAH88). Width fluctuation corrections and giant-dipole resonance energy and width were calculated as described by Lawson and Smith (LS99). The level density parameters and the spin cut-off factor were taken from Gilbert and Cameron (GC65). The remaining parameter in the calculation was the S_0 strength function, which was adjusted to optimize the overall normalization of the calculated results. The latter are compared with the capture cross section of ENDF/B-VI in Fig. 15. The agreement is remarkably good (within a few percent from a few keV to at least several MeV) given the various approximations involved. This agreement supports the validity of the present

measurements and models and also the validity of the ENDF/B-VI capture cross section. It also suggests that discrepancies between the present work and other aspects of ENDF/B-VI are probably substantive.

The differences between evaluated and calculated elastic-scattering cross sections shown in Fig. 13 imply discrepancies within other aspects of the ENDF/B-VI evaluation, probably in the inelastic-scattering area. As noted in Appendix C, the experimental knowledge of ^{197}Au inelastic neutron scattering is not strong, being largely confined to the work of deVilliers et al. (deV+65). However, the first several measured inelastic excitation cross sections can be compared with the corresponding ENDF/B-VI values and the results of the present RCCM calculations. In doing so it is emphasized that the RCCM is only a simple spherical-rotor approximation of a far more complex anharmonic rotational interaction. Such a comparison is shown in Fig. 16. The evaluated excitation of the 77 keV level is in reasonable agreement with the measured values, while the results of RCCM calculations are somewhat lower. This is not surprising as the RCCM treats this excitation function as a compound-nucleus process alone. It is reasonable to expect additional contributions due to direct-reactions not a part of the simple spherical rotational model. The comparisons are quite different for the composite excitations of the 269 and 279 keV levels. In this case the results calculated with the RCCM spherical-rotator approximation approach the measured excitation cross sections, while the comparable evaluated quantities are of much larger magnitude. The latter difference is $\approx \frac{1}{4}$ of a barn, which is a significant portion of the elastic-scattering discrepancy shown in Fig. 13. Similar comparisons can be made for higher excited states but the experimental data is too fragmentary to draw quantitative conclusions.

VII. Summary Remarks

The fast-neutron total cross sections of ^{197}Au are reasonably well known from several-hundred keV to several hundred MeV, as outlined in Appendix A. There are some discrepancies at lower energies and some careful lower-energy measurements are warranted. These are not technically difficult but must be carefully done to avoid experimental perturbations and to achieve good accuracies. The present and very early work by the author and his associates provides very nearly all the experimental knowledge of fast neutron "elastic" scattering from ^{197}Au . However, there is nothing below ≈ 0.3 MeV nor between ≈ 1.5 and 4.5 MeV and, with the exception of a single 14.6 MeV distribution, nothing at all above 10 MeV. Experimental inelastic-scattering cross sections of ^{197}Au seem to be entirely limited to forty year old work by the author and his associates (deV+65). Certainly, some extensive new measurements are in order. High quality scattering measurements are difficult but technologically feasible. The problem is the lack of operable modern facilities and experienced personnel.

^{197}Au is approaching sphericity thus it is not surprising that simple SOMs generated in this work and found in the recent literature (e.g. KD03) are remarkable successful in describing many aspects of the present experimental results. They can provide for many needs of technological applications. They even can be used for more basic investigations

such as the exploration of dispersion properties. It is noted that the SOM potential strengths, expressed in terms of volume-integrals-per-nucleon, are quite reasonable. The real and imaginary SOM potential geometries are quite different., with the imaginary radius being very much larger than the real radius.

The RCCM simple symmetric rotational approximation is very successful in describing many aspects of the fast neutron elastic scattering and total cross sections of ^{197}Au using both full six-parameter fitting and two parameter fitting with the suggested "regional" geometry. It seems clear that the deformations of ^{197}Au are approaching those of a spherical nucleus with $\beta_2 \approx -0.10$ to -0.015 and $\beta_4 \approx -0.01$ to -0.05 .

Dispersion effects are certainly a physical reality that will have an impact on some aspects of basic understanding and model use. However, their application involves a number of approximations, which are not well known. One of these is the energy dependencies of the potential geometries, and another the large extrapolations of the potential-strength energy dependencies. Use of dispersion models does not significantly improve the description of neutron interactions with ^{197}Au at the present time, though it does unify interactions in the bound and unbound energy regions.

The present work, combined with prior studies of the neutron interaction with heavy collective nuclei by the author, has resulted in a "regional" model the geometry of which seems reasonably suitable from at least $A \approx 150$ to 200, with changes in the nuclear structure reflected in potential strengths which appear to vary in a systematic way with mass and collective deformation. The details of this behavior should be filled in and the concept extended through the double-closed-shell region of ^{208}Pb and on into the actinide region.

Aspects of the present work support some portions of the ENDF/B-VI ^{197}Au evaluation (e.g. the total cross section and the higher-energy elastic scattering). Other aspects of the present results are not consistent with the ENDF/B-VI evaluation.

Over the last several decades there have been large technological advances in computing power, putting at one's desk computational capability that formerly was available only at large institutional computing facilities, if there. Unfortunately, these technological advances have not generally been matched by nuclear modeling capability. In the context of the present considerations, the author does not know of a coupled-channels computational fitting code that will handle an asymmetric-rotational model of the fast neutron interaction, including direct and compound-nucleus processes and experimental fitting, analogous to that of the SOM. If one considers increasingly heavier targets one must also deal with fission. Such a computational tool must be developed and much improved experimental data obtained before the above considerations can be significantly improved.

Acknowledgements

The author is indebted to Drs. F. Kondev, J. Raynal, and P. Young for comment and advice in the context of this paper and more generally over many years. He is also indebted to the staff of the National Nuclear Data Center, Brookhaven National Laboratory and personnel at the Argonne Natl. Lab. Library for making it possible to obtain a wealth of experimental data and technical information reported in the literature. Finally, the provision of advanced computing systems by Mr. John Bölling and associates is gratefully acknowledged.

References

- But+82, Butz-Jorgensen, C. et al., 1982, *Z. Phys.* **A360**, 265.
Chi+92, Chiba et al., 1992, *Phys. Rev.* **C45**, 1260.
CL55, Cranberg, L. and Levin, J., 1955, *Proc. Conf. on Peaceful Uses of Atomic Energy*, Geneva, United Nations Press.
CSL83, Conde, H., Smith, A. and Lorenz, A., 1983, IAEA Tech Report **IAEA-227**.
deV+65, deVilliers, J. et al., 1965, *Z. Phys.* **183**, 323.
DF58, Davydov, A. and Filippov, G., 1958, *Nucl. Phys.* **8** 237.
Dro87, Drosig, M. 1987, IAEA Report, **IAEA-TECDOC-410**.
ENDF ENDF/B-VI, Available from the National Nuclear Data Center, Brookhaven National Laboratory.
Fes58, Feshbach, H., 1958, *Ann. Rev. Nucl. Sci.* **8** 49.
FPW54, Feshbach, H., Porter, C. and Weisskopf, V., 1954, *Phys. Rev.* **96** 448.
GC65, Gilbert, A. and Cameron, A., 1965, *Can. Jour. Phys.* **43** 1446.
Han+85, Hansen, L. et al., 1985, *Phys. Rev.* **31** 111.
Hod63, Hodgson, P., 1963, *The Optical Model of Elastic Scattering* Clarendon, Oxford.
HS62, Hecht, K. and Satchler, G., 1962, *Nucl. Phys.* **32** 286.
JLM77, Jeukenne, J., Lejeune, A. and Mahaux C., 1977, *Phys. Rev.* **C16** 80.
KD03, Koenig, A. and Delaroche, J., 2003, *Nucl. Phys.* **A713** 231.
Lan61, Lane, R. et al., 1961, *Ann. Phys.* **12** 135.
Lan62, Lane, A., 1962, *Nucl. Phys.* **35** 676; also 1962, *Phys. Rev. Lett.* **8** 171.
LGS87, Lawson, R., Guenther, P. and Smith, A., 1987, *Phys. Rev.* **C36** 1287.
Lip66, Lipperheide, R., 1966, *Nucl. Phys.* **89** 87.
LS99, Lawson, R. and Smith, A., 1999, Argonne Natl. Lab Reports **ANL/NDM-145** and **ANL/NDM-148**.
LS01, Lawson, R. and Smith, A., 2001, Argonne Natl. Lab, Report **ANL/NDM-151**.
MDH81, Mughabghab, S., Divadeenam, M. and Holden, N., 1981, *Neutron Cross Sections* Academic Press, New York
MN59, Mottelson, B. and Nilsson, S., 1959, *K. Danske Vidensk. Selsk. mat. Fys. Skr.* **1** 8.
MNS95, Moller, P., Nix, J. and Swiatecki, W., 1995, *At. Data and Nucl. Data Tables* **59** 185.
Mol80, Moldauer, P., 1980, *Nucl. Phys.* **A344** 185.

- MY87, Macklin R. and Young, P., 1987, Nucl. Sci. and Eng. 97 239.
 NDS95, Chunmei, Z., 1995, Nucl. Data Sheets 76 399.
 Pas57, Passatori, G., 1967, Nucl. Phys. A95 694.
 Pre62, Preston, M., 1962, **Physics of the Nucleus**, Addison-Wesley, Reading, MA.
 Ray95, Raynal, J., 1995, CEA Report CEA-N-2772; also private communication.
 Sat83, Satchler G., 1983, **Direct Nuclear Reactions** Addison-Wesley, Reading, Ma.
 SGS77, Smith, A., Guenther, P. and Sjoblum, R., 1977. Nucl. Instr. Meth. 140, 397.
 SG92, Smith, A. and Guenther, P., 1992, Argonne Natl. Lab. Report ANL/NDM-127.
 Smi+67, Smith, A., et al., 1967, Nucl. Instr. Meth., 50, 277.
 Smi91, Smith, A., 1991, Argonne Natl. Lab. memorandum, unpublished.
 Smi00, Smith, A., 2000, Argonne Natl. Lab. Report, ANL/NDM-151; also 2001. Ann. Nucl. Energy 28 1745.
 Smi01, Smith, A., 2001, Argonne Natl. Lab. Report, ANL/NDM-153; also 2002, Ann. Nucl. Energy 29 1241.
 Smi03, Smith, A., 2003, Argonne Natl. Lab. Report, ANL/NDM-155; also 2004, J. Phys. G30 407
 Smi04, Smith, A., 2004, Argonne Natl. Lab. Report, ANL/NDM-157, also 2004, Ann. Nucl. Energy 31 1831;
 Smi05, Smith, A., 2005, Argonne Natl. Lab. Report, ANL/NDM-160, also 2005, Ann. Nucl. Energy, in press.
 Tul90, Tuli, J., 1990, Nuclear Wallet Cards, Available from the National Nuclear Data Center, Brookhaven Natl. Lab.
 Vie+78, Vieu, Chu et al., 1978. J. Phys. G4 531.
 WAH88, Wapstra, A, Audi, A. and Hoekstra, R., 1988, At. Data and Nucl. Data Tables 39 281.
 WG85, Walter, R. and Guss, P., 1985, **Proc. Conf. on Nucl. Data for Basic and Applied Sci.** Eds. Young, P. et al., 2 272.
 Wol51, Wolfenstein, L., 1951, Phys. Rev. 82 690.
 YA87, Young, P. and Arthur, E., 1987, Los Alamos Natl. Lab. Report LA-10915 -pr31.

Appendix A. ¹⁹⁷Au Neutron Total Cross Section Database

CINDA-EXFOR was examined to determine the resources of ¹⁹⁷Au experimental neutron total cross section data above $\approx 50 - 100$ keV. There were 19 references, as per the following. The average age is 37 years.

- Abf+01, Abfalter, W. et al., 2001, Phys. Rev. C63 0446, $\approx 5 - 550$ MeV, #13753.
 Age+50, Ageno, M. et al., 1950, Nuvo. Cem. 10 281, ≈ 14 MeV. #21263.
 Bra+58, Bratenahl, A. et al., 1958, Phys. Rev. 110 927, $\approx 7 - 14$ MeV, #11155.
 Con58, Conner, J., 1958, Phys. Rev. 109 1268, $\approx 13 - 16$ MeV, #11320.
 Coo+52, Coon, J. et al., 1952, Phys. Rev. 88 562, ≈ 14 MeV, #11056.
 Day65, Day, R., private communication to NNDC, $\approx 0.5 - 4$ MeV, #12191.
 FG71, Foster, D. and Glasgow, D., 1971, Phys. Rev. C3 576, $2 - 15$ MeV, #10047.

- Lar+81, Larsen, D. et al., 1981, Oak Ridge Natl. Lab. Report, **ORNL-5786**, $\approx 2 - 80$ MeV, #12882.
- ND54, Nereson, N. and Darden, S., 1954. Phys. Rev. **94** 1678, $\approx 2.8 - 13$ MeV, #11308.
- Pet+60, Peterson, J. et al., 1960, Phys. Rev. **120** 521, $\approx 17 - 29$ MeV, #11108.
- Poe81, Poenitz, W. et al., 1981, Nucl. Sci. and Eng. **78** 333, $\approx 0.05 - 5$ MeV, #10935.
- Pur+94, Purtov, O. et al., 1994, Atom. En. **77** 44, $\approx 0.002 - 0.5$ MeV, #41175.
- PW83, Poenitz, W. and Whalen, J., Argonne Natl. Lab. Report **ANL/NDM-80**, $\approx 2 - 20$ MeV, #11540.
- Set65, Seth, K. et al., 1965, Phys. Lett. **16** 306. $\approx 0.05 - 0.65$ MeV, #11781.
- SW53, Snowdon, C. and Whitehead, W., 1953. Phys. Rev. **90** 615, $\approx 0.1 - 0.7$ MeV, #11559.
- Wal+53, Walt, M. et al., 1953, Phys. Rev. **89** 1271, $\approx 1 - 3$ MeV, #11746.
- WB55, Walt, M. and Beyster, J., 1955, Phys. Rev. **98** 677, ≈ 4 MeV, #11215.
- WM66, Whalen, J. and Meadows, J., 1966, Argonne Natl. Lab. Report, **ANL-7210**, $\approx 0.1 - 0.7$ MeV, #11540.
- Wis+98, Wisshak, K. et al., 1998, Phys. Rev. **C57** 391, $\approx 0.01 - 0.2$ MeV, #22388.

Denotes EXFOR number.

Only six of these works were carried out in the last quarter century, and most of the information comes from the above references FG71, Lar+81, Poe+81, PW83 and Abf01. All of the above experimental data was combined into one file that consisted of ≈ 2100 cross sections. This combined file was then culled for obviously erroneous results, ordered by energy and averaged over 50 keV increments below 0.5 MeV, over 100 keV increments from 0.5 to 5.0 MeV, over 200 keV at higher energies. The averaging weighted the individual values using the uncertainties assigned to the various data values by the authors. When those were not available, or suspicious, the author introduced his estimate of the uncertainties. The resulting energy-ordered and averaged total cross sections are shown in Fig. A-1. This figure shows portions of the same data in three energy windows, A) 0 - 500 MeV, B) 0 - 100 MeV, and C) 0 - 20 MeV. The uncertainties reflect those of the various data sets, combined in quadrature. This ordered and averaged set of neutron total cross sections constructed from the literature as is used throughout the above text.

Appendix B. ¹⁹⁷Au Neutron Elastic-Scattering Database

CINDA-EXFOR was also examined to determine the resources of experimental fast-neutron "elastic"-scattering data relevant to the present considerations ($\approx \geq 0.1$ MeV incident energies and with reasonable angle and energy definition and resolutions). The corresponding data as given in the EXFOR files were then assembled. The results consisted of only eleven data sets, as outlined below. Some of these data sets were not used due to lack of relevance to the present considerations.

- All+56, Allen, R. et al., 1956, Phys. Rev. **104** 731, A ≈ 0.5 MeV distribution, #12207.
- BHB66, Buccino, S., Hollandsworth, C. and Bevington, P., 1966, Z. Phys. **196** 103, 5 MeV distribution, #11877.
- CC72, Cox, S. and Cox, E., 1972, Argonne Natl. Lab. Report ANL-7935, 0.88 MeV distribution, #10332.
- Day65, Day, R., 1965, private communication to the NNDC, distributions at 0.5, 1.0 and 2.5 MeV, #12191.
- deV65, deVilliers, J. et al., 1965, Z. Phys. **183** 323, About 24 distributions distributed between ≈ 0.3 and 1.5 MeV. This is the primary block of data available in the literature; it was augmented by private files of the author and used in this work as described in the body of the text, #12240.
- Eta73, Etamad, M., 1973, Report AE-482, ≈ 7 MeV distribution, #20436.
- Han+88, Hansen, L. et al., 1988, Phys. Rev. **C31** 111, distribution at 14.6 MeV. #12935.
- HW71, Holmqvist, B. and Wiedling, T., 1971, Report AE-430, 8 MeV distribution, #20162.
- Kir+68, Kirchnir, F. et al., 1968, Phys. Rev. **176** 1405, A number of distributions at small scattering angles (few degrees or less). Not relevant to the present work, #11977.
- WB54, Walt, M. and Barschall, H., 1954, Phys. Rev. **93** 1062. An ≈ 1.0 MeV distribution, #11637.
- WB55, Walt, M. and Beyster, R., 1955, Phys. Rev. **98** 677, ≈ 4.1 MeV distribution, #11215.

Again, “#” denotes an EXFOR number.

Only one of these citations is less than thirty years old, and then provides only a single ≈ 14.6 MeV distribution. Only one set (deV+65) covers an extended energy range in detail. Only one or two of the citations report true “elastic” processes free of inelastic scattering contributions. These are generally very limited and elderly references. They and the present work are apparently all that is known of fast-neutron elastic scattering from one of the more important neutron standards — ^{197}Au ! This is an embarrassing situation at best.

Appendix C. ^{197}Au Neutron Inelastic-scattering Database.

There are only twelve CINDA-SCISRS citations to inelastic neutron scattering from ^{197}Au , as outlined in the references below. Of these, only reference (deV+65) is very relevant to the present considerations and it is forty years old!

- Aki+74, Akiyoshi, T. et al., 1974, Nucl. Sc. Tech. (Japan) **11** 523, 14 MeV results, #21588.
- Bor+67, Borman, M. et al., 1967, Report EANDC-76, 14 MeV continuum results, #21503
- Bor+68, Bornemisza, P. et al., 1968, AK **10** 112, isomer cross sections, #30338.

- BSA92, Baggaid, M., Siad, M., andl Allab. M., 1992, JRN/L 166 493, metastable activities at 14 MeV incident energies, #31524.
- deV+65, deVilliers, J. et al., 1965. Z. Phys. 183 323, excitations from 0.3 to 1.5 MeV, #12240.
- DK68, Durant, S. and Koehler, W., 1968, J. Nucl. Energ. 22 632, fission=spectrum average values, #11985.
- JG73, Janczyn, J. and Gorski, L., 1973, JRC 14 201, isomer values at 14 MeV, #30322.
- OOO79, Oezek, F, Oezyol, H. and Ortaovali, A., 1979, Phy. Rev. Lett. 41 87, 3 and 14 MeV isomer values, #11985.
- MDT54, Marten, H., Diven, B. and Taschek, R., 1954, Phys. Rev. 93 199, metastable values, #11985.
- Pet+68, Peto, G. et al., 1968, AHP 25 91, 14 MeV activation, #30069.
- Pro80, Prokopets, G., 1980, YF 32 19, continuum spectra measurement at 20 MeV incident. #41102
- Pet+73, Peto, G. et al., 1973, AHP 33 363, Pu(α ,n)Be source, #30265.

again denotes EXFOR number.

Tables

Table 1. SOM parameters. Energies and potential depths are in MeV, geometries in fermis, and strengths in volume-integrals-per-nucleon (J_i , in units of $\text{MeV}\cdot\text{fm}^3$).

Real Potential

Depth

$$V = 48.522 - 0.2244 \cdot E$$

$$J_V = 394.02 - 1.8222 \cdot E$$

Reduced radius

$$r_V = 1.2073$$

Diffuseness

$$a_V = 0.7129$$

Imaginary Potential

Depth

$$W = 4.7387 + 0.3141 \cdot E$$

$$J_W = 25.99 + 1.723 \cdot E$$

Reduced radius

$$r_W = 1.3548$$

Diffuseness

$$a_W = 0.3438$$

Spin - Orbit Potential (Walter and Guss (WG85))

Depth

$$V_{so} = 6.613 - 0.015 \cdot E$$

$$r_{so} = 1.103$$

$$a_{so} = 0.560$$

Table 2. RCCM parameters deduced from six parameter fitting. Energies and potential depths in MeV, potential strengths in volume-integrals-per nucleon (J_i , in MeV-fm³), geometries in fermis.

Real Potential

Depth

$$V = 45.213 - 0.1736 \bullet E$$

$$J_V = 416.58 - 1.5995 \bullet E$$

Reduced Radius

$$r_V = 1.2614$$

Diffuseness

$$a_V = 0.6753$$

Imaginary Potential

Depth

$$W = 4.1454 + 0.9200 \bullet E$$

$$J_W = 14.97 + 3.3223 \bullet E$$

Reduced Radius

$$r_W = 1.3322$$

Diffuseness

$$a_W = 0.2345$$

Spin-Orbit Potential as per Table 1.

Deformations

$$\beta_2 = -0.131$$

$$\beta_4 = -0.031$$

Table 3. RCCM parameters deduced from two parameter fitting. Energies and potential depths in MeV, potential strengths in volume-integrals-per-nucleon (J_i , in $\text{MeV}\cdot\text{fm}^3$), geometries in fermis.

Real Potential

Depth

$$V = 45.750 - 0.1839 \cdot E$$

$$J_V = 410.97 - 1.6520 \cdot E$$

Reduced Radius

$$r_V = 1.2568 \text{ fixed}$$

Diffuseness

$$a_V = 0.6292 \text{ fixed}$$

Imaginary Potential

Depth

$$W = 2.0834 + 0.57834 \cdot E$$

$$J_W = 14.07 + 3.8922 \cdot E$$

Reduced Radius

$$r_W = 1.2692 \text{ fixed}$$

Diffuseness

$$a_W = 0.4785 \text{ fixed}$$

Spin-Orbit Potential as per Table 1.

Deformations

$$\beta_2 = -0.100$$

$$\beta_4 = -0.031$$

Table 4. Dispersive spherical optical model parameters, case DISP-A. Energies and potential depths in MeV, potential strengths (J_i) in volume-integrals-per-nucleon (in $\text{MeV}\cdot\text{fm}^3$), geometries in fermis.

Real potential

Depth

$$V = 50.363 - 0.24171 \cdot E$$

$$J_V = 356.94 - 1.7131 \cdot E$$

Reduced radius

$$r_V = 1.1479$$

Diffuseness

$$a_V = 0.7097$$

Imaginary potential

Depth

$$W = 3.1304 + 0.5500 \cdot E$$

$$J_W = 13.31 + 4.228 \cdot E$$

Reduced radius

$$r_W = 1.3257$$

Diffuseness

$$a_W = 0.2788 + 0.0086 \cdot E$$

Spin-Orbit Potential (as per table1)

Dispersion fraction

$$\text{DISP} = 1.0277 - 0.0521 \cdot E + 0.00067 \cdot E^2$$

Table 5. Dispersive spherical optical model parameters, case DISP-B. Energies and potential depths are in MeV, potential strengths J_i in volume-integrals-per-nucleon ($\text{MeV}\cdot\text{fm}^3$), geometries in fermis.

Real Potential

Depth

$$V = 49.678 - 0.1333 \cdot E$$

$$J_V = 359.82 - 0.9265 \cdot E$$

Reduced radius

$$r_V = 1.1576$$

Diffuseness

$$a_V = 0.7261$$

Imaginary Potential

Depth

$$W = 6.4455 + 0.1857 \cdot E$$

$$J_W = 19.87 + 3.062 \cdot E$$

Reduced radius

$$r_W = 1.3422$$

Diffuseness

$$a_W = 0.1977 + 0.01572 \cdot E$$

Spin-Orbit Potential (as per Table 1)

Dispersion fraction

$$\text{DISP} = 0.8279 - 0.0549 \cdot E + 0.00025 \cdot E^2$$

Table 6A. The "Regional" potential described in the text and as referenced. All strengths (J_i) are in volume-integrals-per-nucleon ($\text{MeV}\cdot\text{fm}^3$).

Target	Z	A	η	β_2	J_I	ref.
Eu	63	152.0	0.171	0.160	$J_V = 455.95 - 3.147 \bullet E$ $J_W = 20.0 + 3.846 \bullet E$	YA87
Gd	64	157.3	0.186	0.300	$J_V = 434.44 - 0.796 \bullet E$ $J_W = 25.9 + 2.453 \bullet E$	Smi04
Gd	64	157.3	0.186	0.300	$J_V = 434.81 - 2.059 \bullet E$ $J_W = 17.4 + 2.708 \bullet E$	YA87
Ho	67	164.9	0.188	0.300	$J_V = 444.39 - 3.558 \bullet E$ $J_W = 22.4 + 2.151 \bullet E$	Smi00
Ho	67	164.9	0.188	0.300	$J_V = 449.97 - 3.125 \bullet E$ $J_W = 25.5 + 2.363 \bullet E$	YA87
Hf	72	178.5	0.191	0.287	$J_V = 457.15 - 2.593 \bullet E$ $J_W = 19.5 + 2.419 \bullet E$	Smi01
Ta	73	181.0	0.193	0.269	$J_V = 441.08 - 2.463 \bullet E$ $J_W = 16.6 + 3.166 \bullet E$	Smi05
Re	75	186.2	0.194	0.220	$J_V = 428.94 - 3.189 \bullet E$ $J_W = 18.3 + 2.258 \bullet E$	Smi03
Re	75	186.2	0.194	0.220	$J_V = 432.71 - 2.780 \bullet E$ $J_W = 16.5 + 4.931 \bullet E$	MY87

Average values of the above strengths are: -

$$J_V = 442.16 (\pm 1\%) - 2.6344 (\pm 10\%) \bullet E$$

$$J_W = 20.233 (\pm 6\%) + 2.9247 (\pm 9\%) \bullet E$$

The present RCCM results in:-

$$\text{Au } 79 \quad 197.0 \quad 0.198 \quad -0.131$$

$$J_V = 410.97 - 1.652 \bullet E$$

$$J_W = 14.07 + 3.892 \bullet E$$

Table 6B. Averaged "Regional" potential parameters as described in the text.

Real Potential

$$V = 49.5525 - 0.29523 \cdot E \text{ (MeV)}$$

$$r_V = 1.2568 \text{ (fm)}$$

$$a_V = 0.6292 \text{ (fm)}$$

Surface-Imaginary Potential

$$V = 3.069 + 0.4436 \cdot E \text{ (MeV)}$$

$$r_W = 1.2629 \text{ (fm)}$$

$$a_W = 0.4785 \text{ (fm)}$$

Spin-Orbit Potential (as per Table 1)

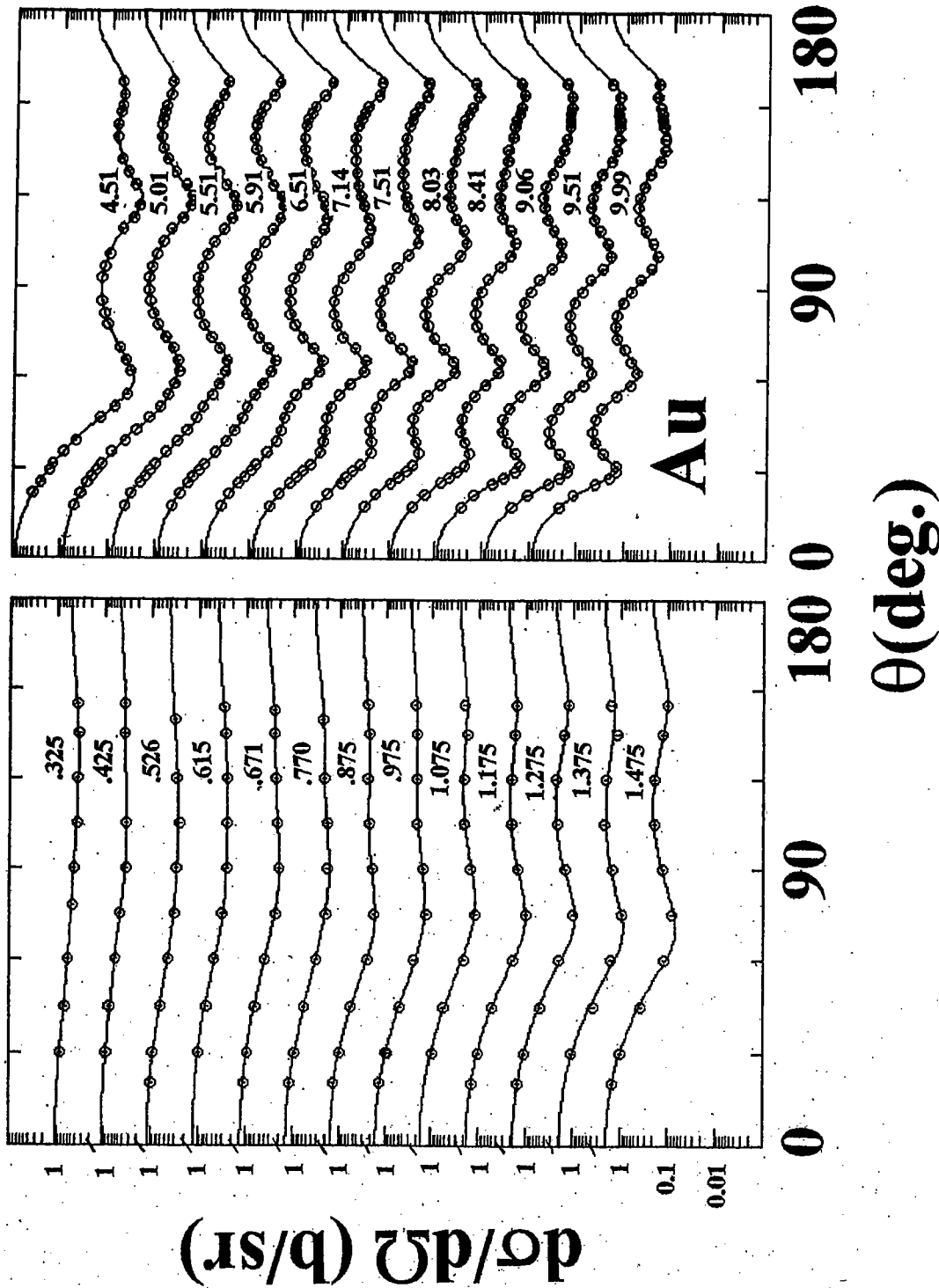


Fig 1. Differential "elastic" scattering cross sections of ^{197}Au . The right panel illustrates the present results. The left panel shows energy averages the earlier lower-energy work of the author and his associates (de V+65). Symbols indicate the experimental values as described in the text, and curves the results of fitting them with legendre-polynomial series. Incident energies are numerically given in MeV. Throughout this work angle-differential results are presented in the laboratory coordinate system.

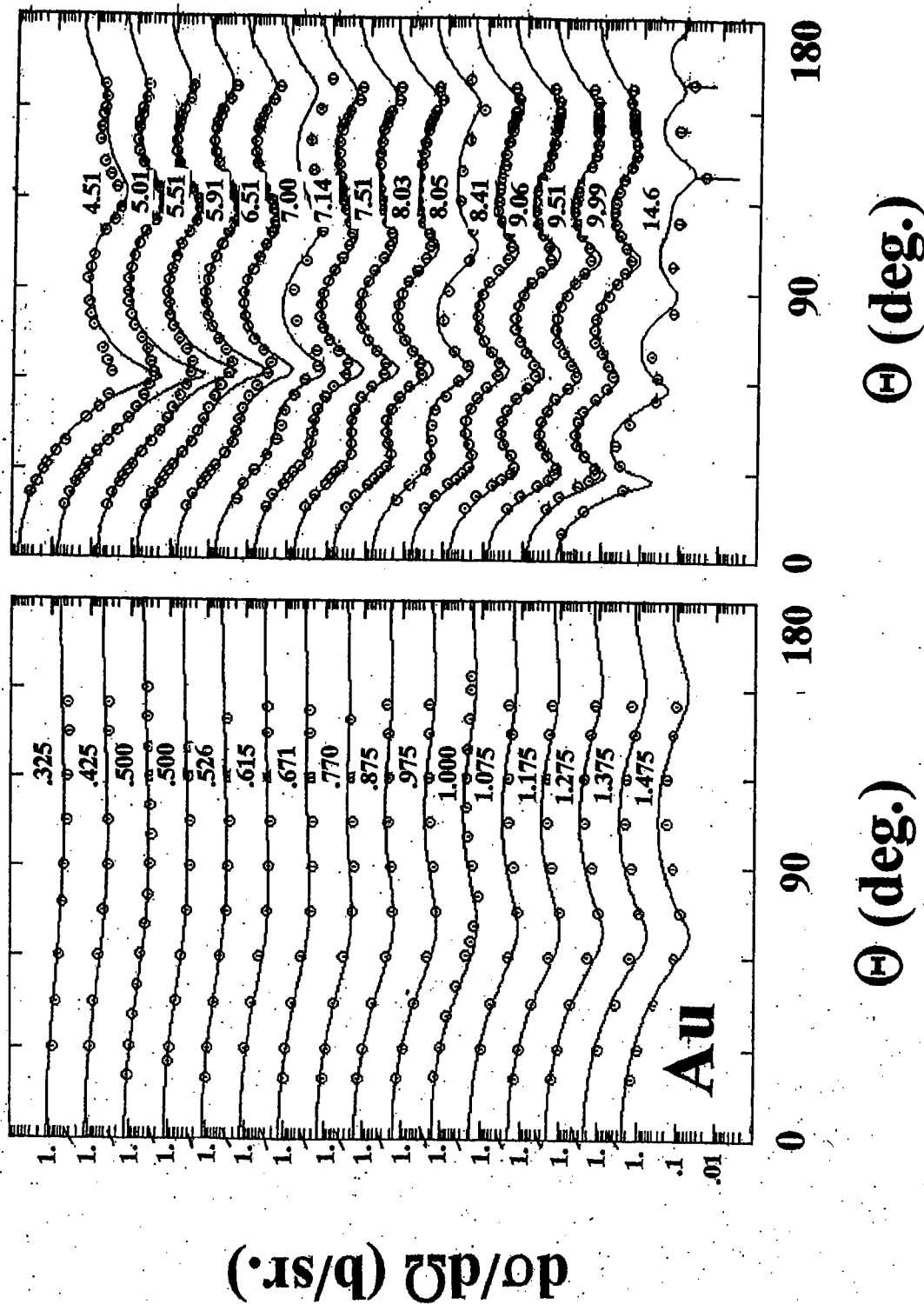


Fig. 2. Measured (symbols) and calculated (curves) differential elastic-scattering cross sections of ^{197}Au . The calculations used the SOM parameters of Table 1. Incident neutron energies are numerically noted in MeV.

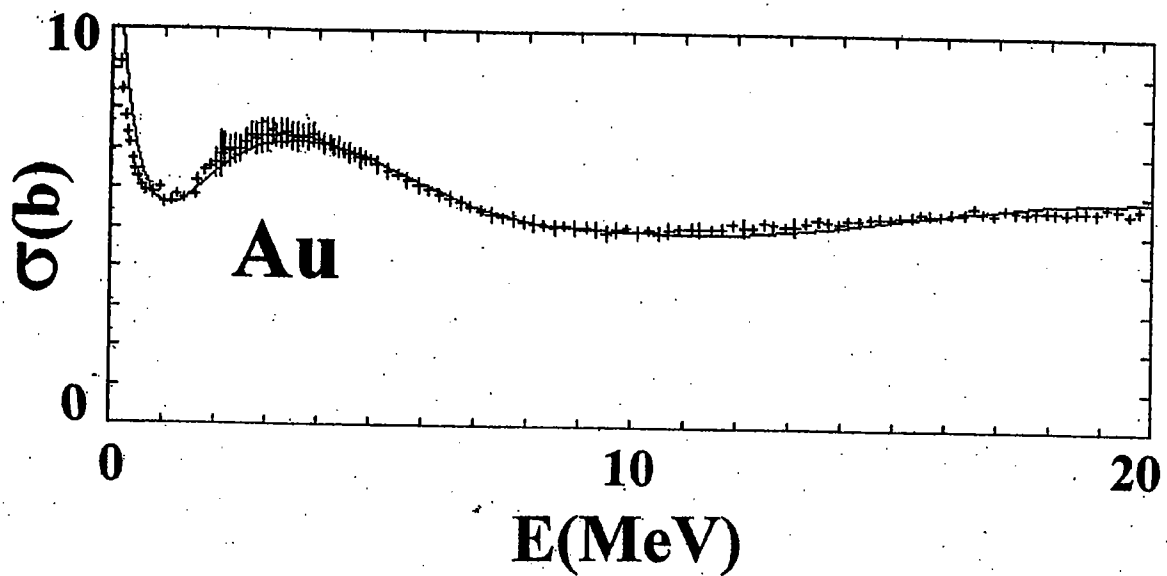


Fig. 3. Measured and calculated neutron total cross sections of ^{197}Au . The calculations used the SOM model parameters of Table 1. The ordered and averaged experimental values of Appendix A are indicated by "+" symbols and the calculational result by the simple curve.

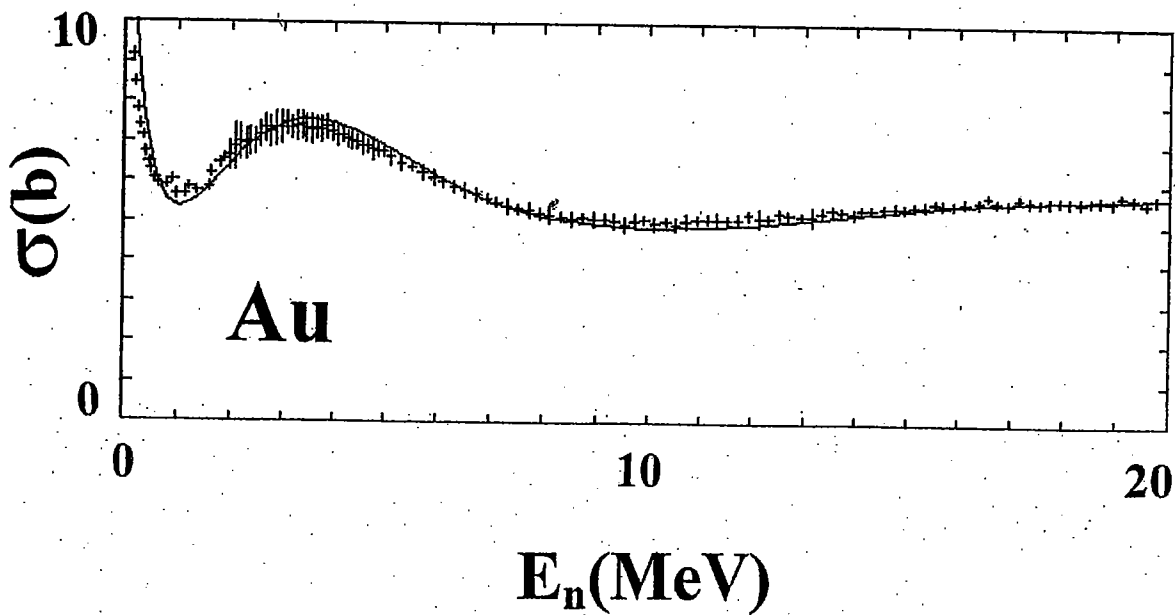
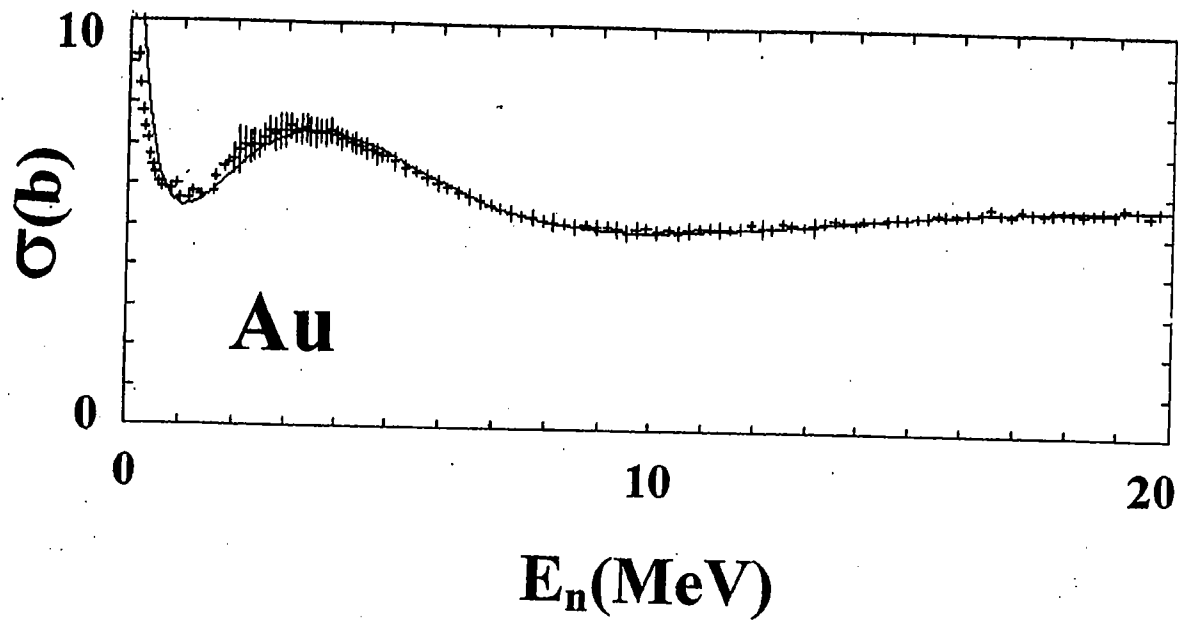


Fig. 4. Comparisons of measured (symbols) and RCCM calculated (curves) neutron total cross sections of ^{197}Au . The experimental data is defined in Appendix A. The upper-panel calculations are based upon the potential of Table 3. The lower-panel calculations are based upon the potential of Table 2.

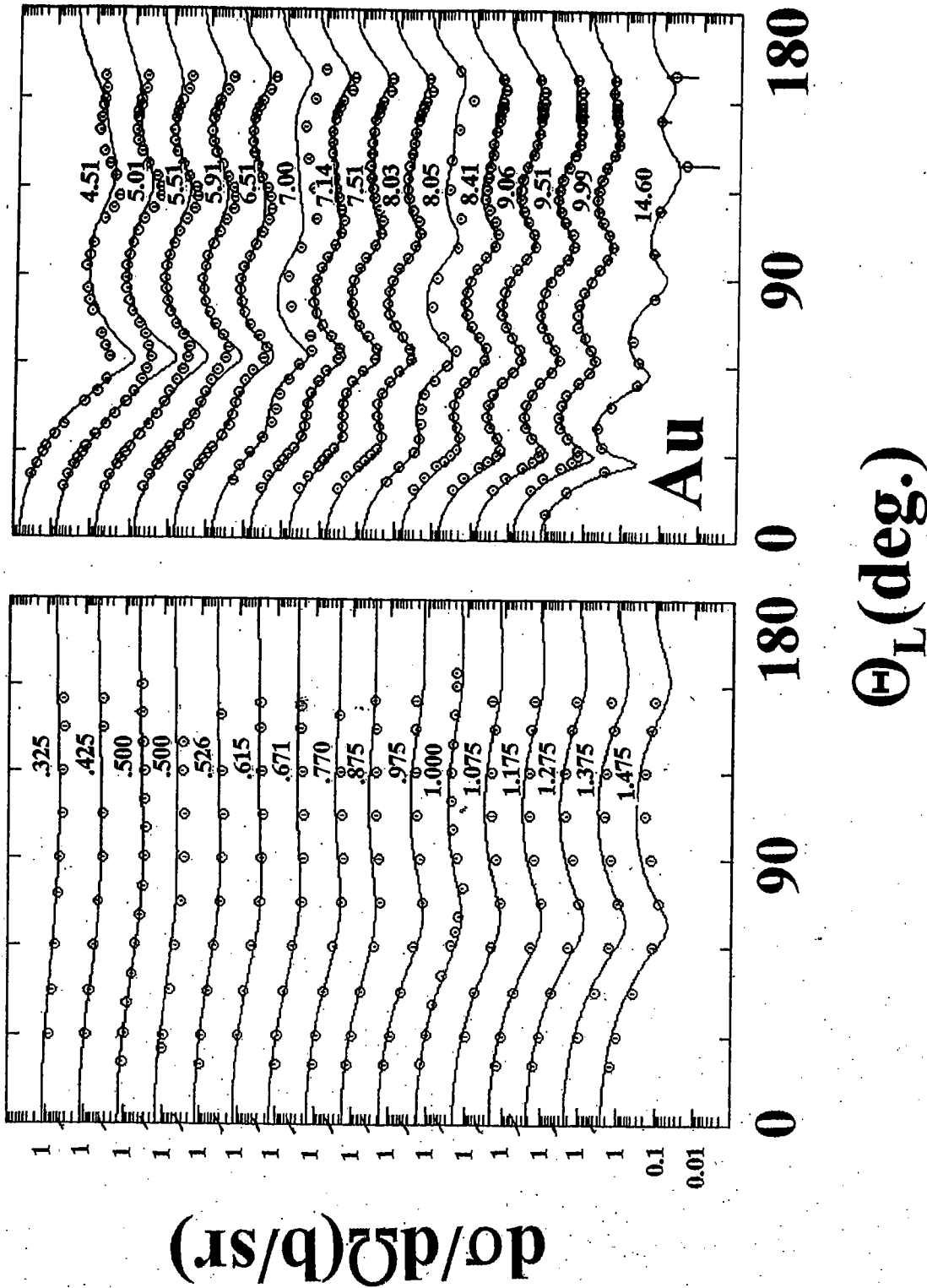


Fig. 5. Comparison of measured (symbols) and calculated (curves) differential "elastic" scattering cross sections of ^{197}Au . The nomenclature is identical to that of Fig. 2. The calculations used the two-parameter potential of Table 3.

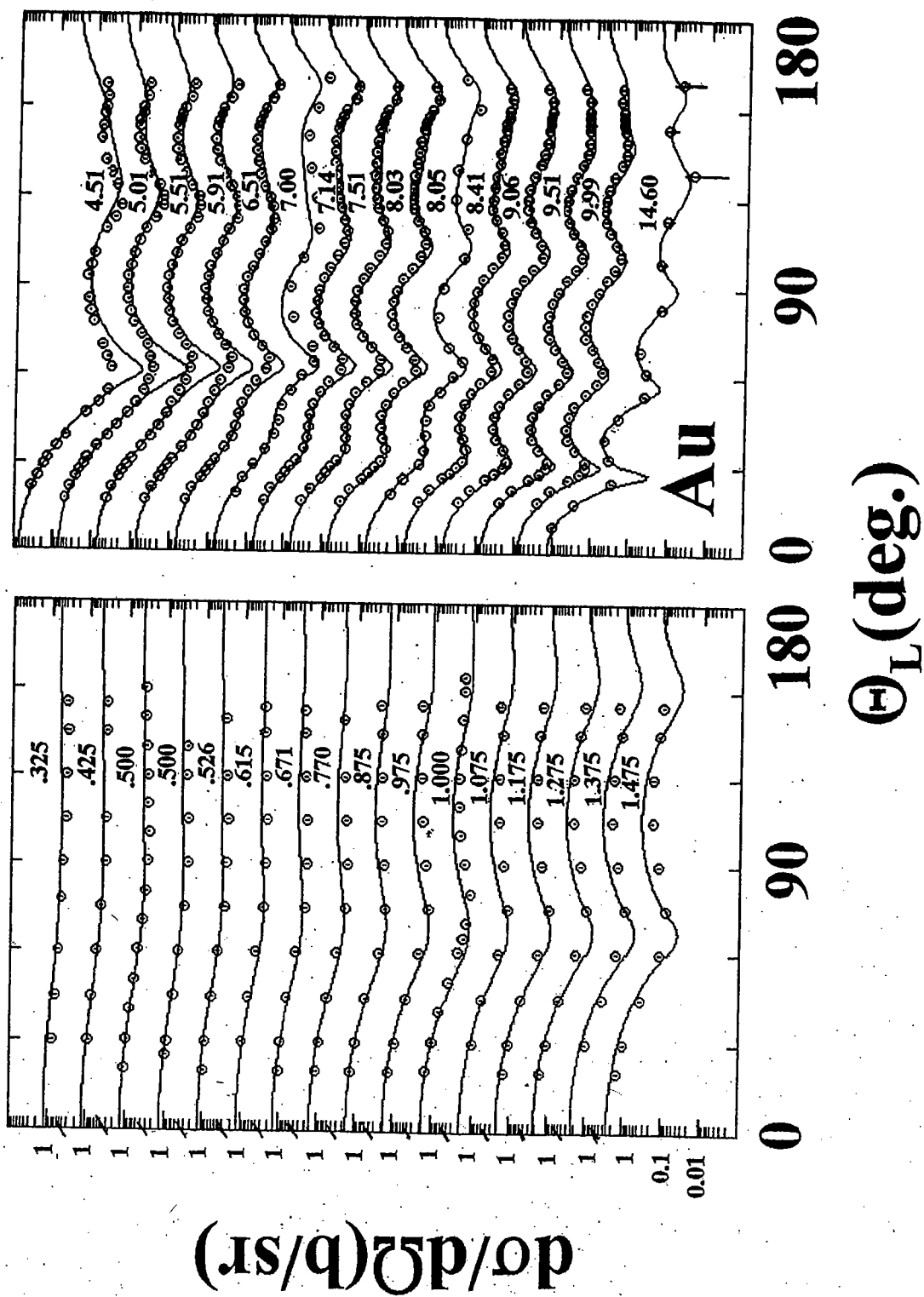


Fig. 6. The nomenclature is identical to Fig. 5, except that the calculations used the potential of Table 2.

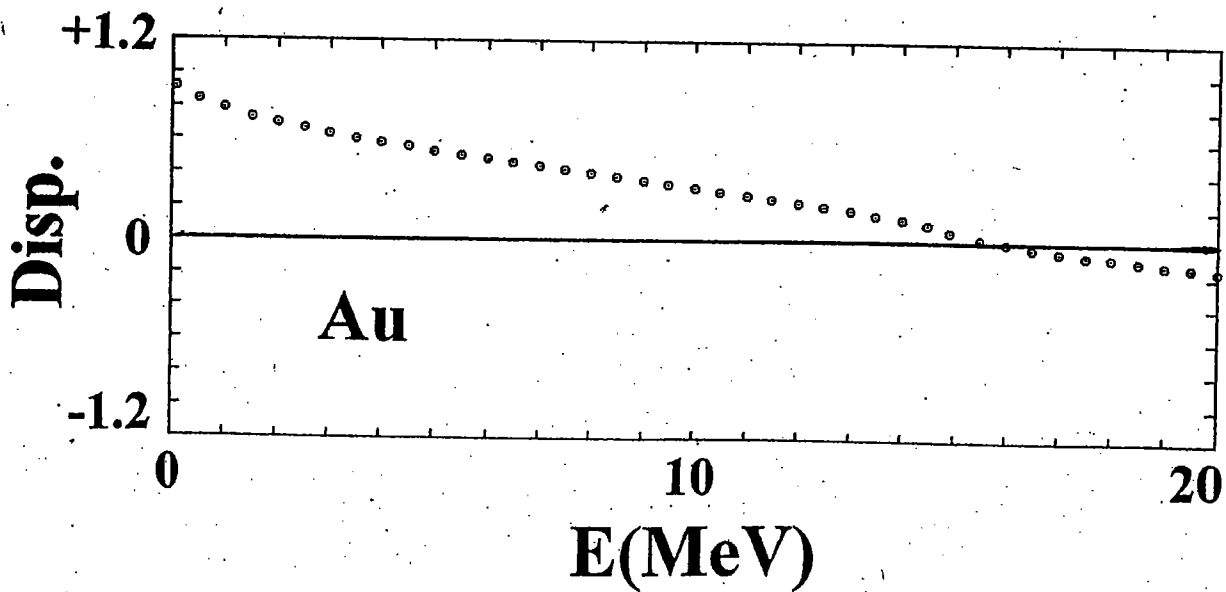
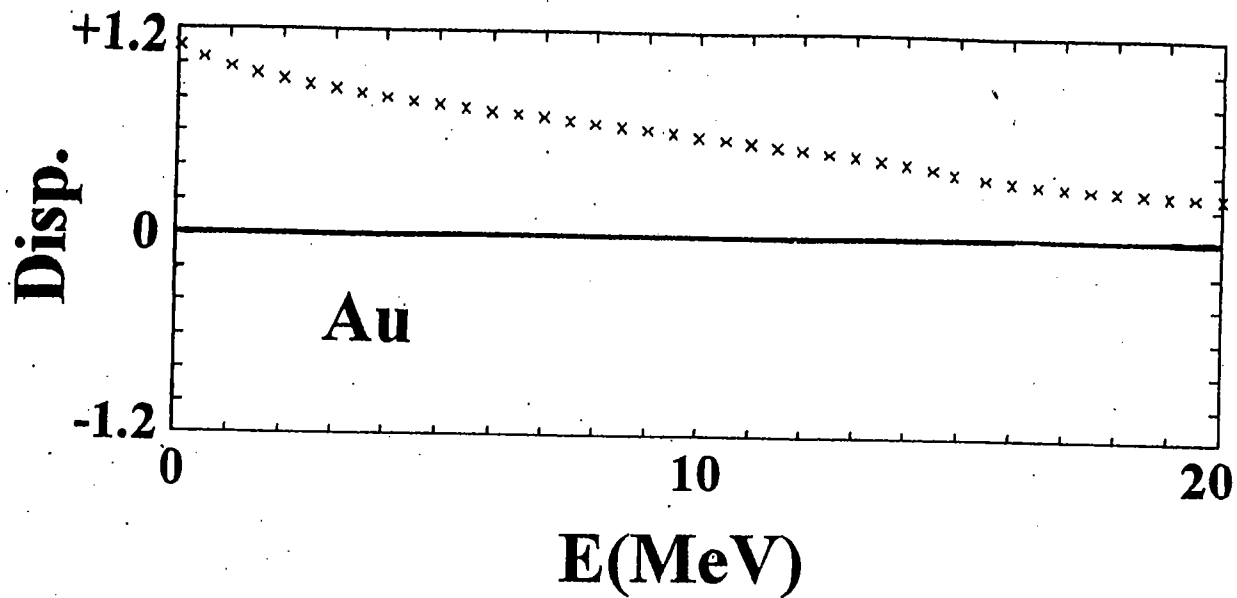


Fig. 7. Dispersion fractions as a function of incident energy. The upper panel shows the results obtained with the extrapolation of DISP-A while the lower panel shows the values obtained with the extrapolation of DISP-B of the text.

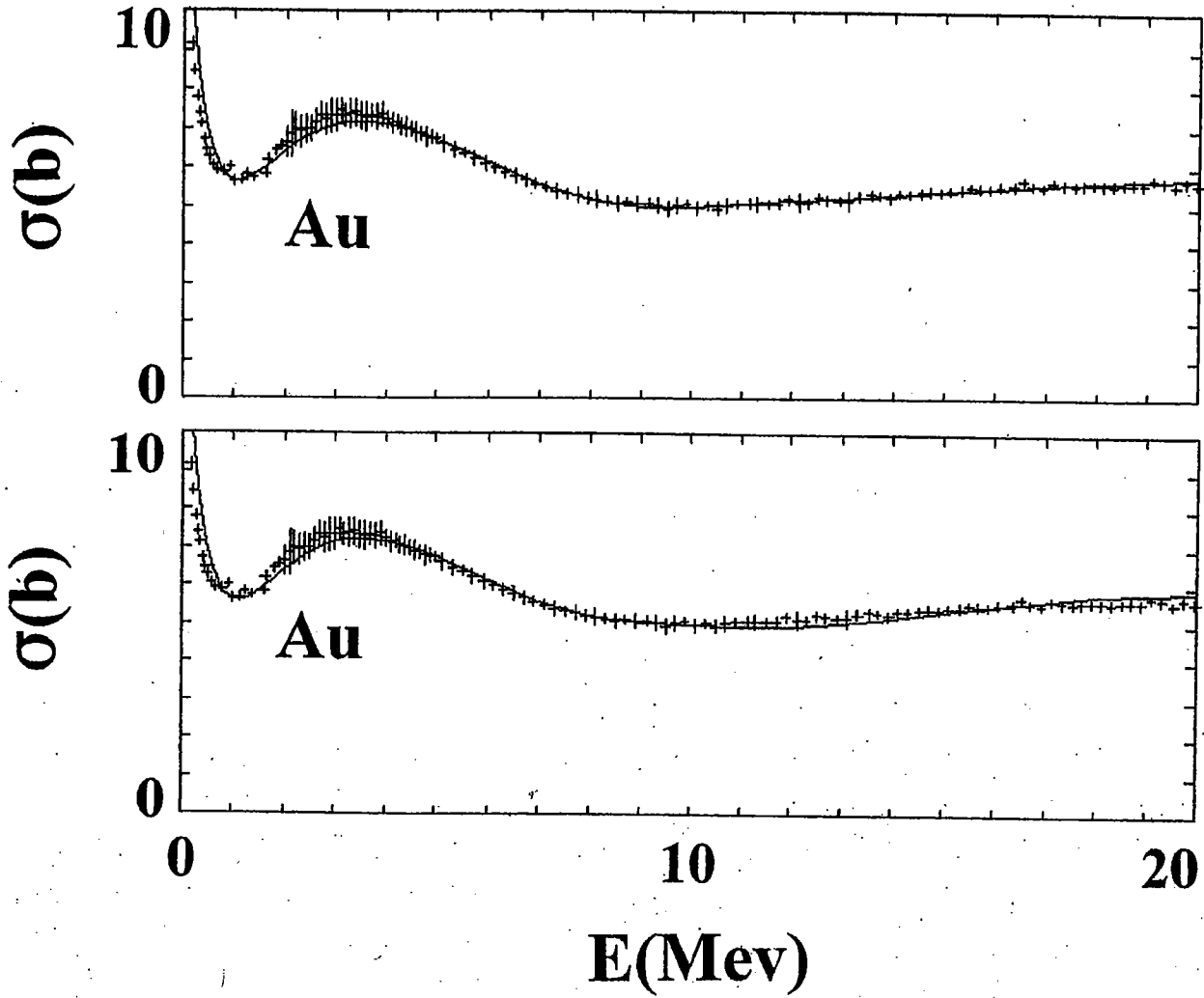


Fig. 8. Illustration of the effect of the dispersion fraction on ^{197}Au total cross sections. The upper panel illustrates the results obtained by fitting using the DISP-B DOM, and the lower panel illustrates the same quantities obtained with the SOM without any DISP contribution.

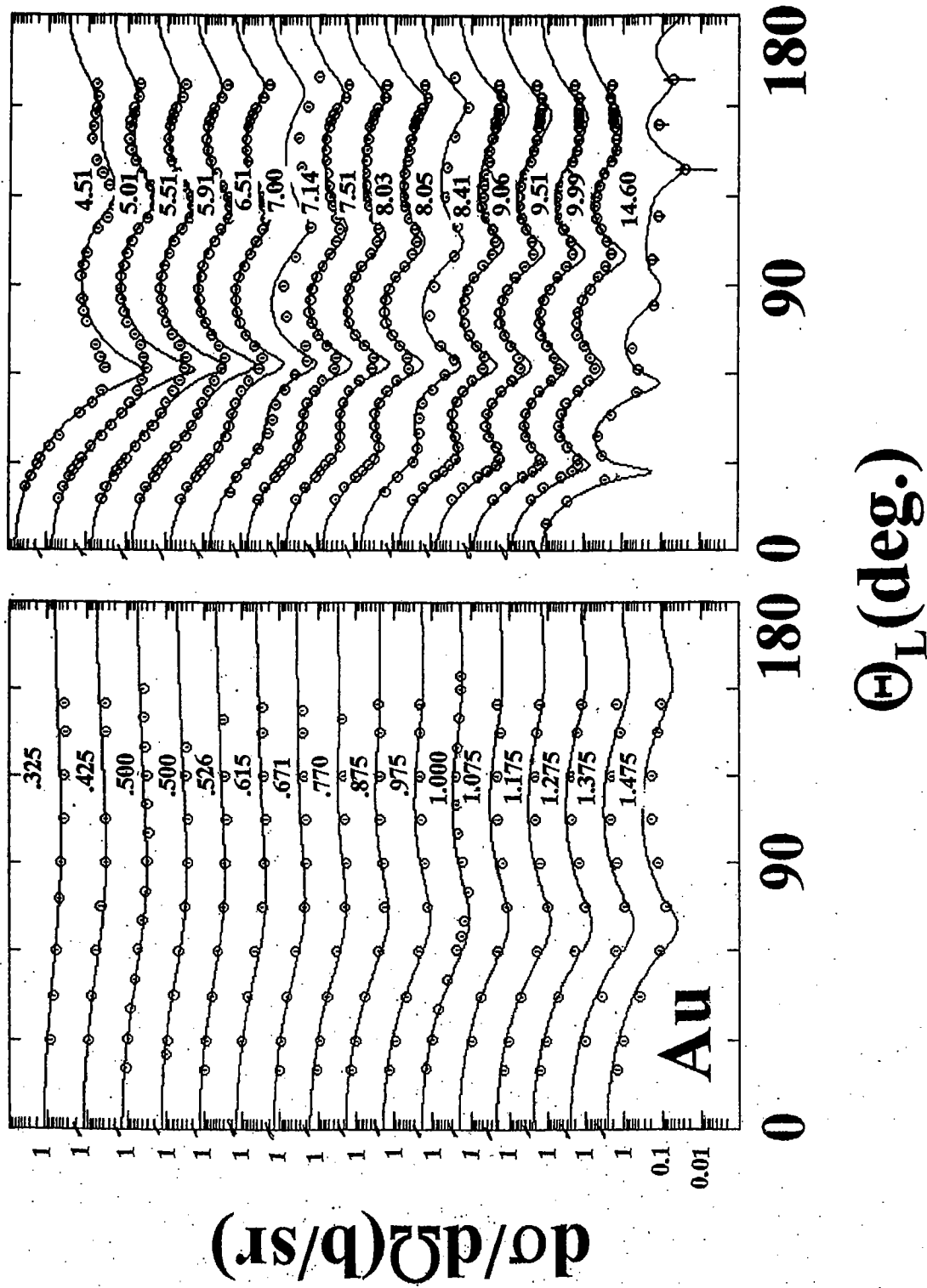


Fig. 9. Comparison of measured (symbols) and calculated (curves) "elastic" scattering cross sections of ¹⁹⁷Au. The measured values are identical to those shown in Fig. 2. The curves were obtained using the DISP-B potential of Table 4. Essentially the same comparison was obtained using the DISP-A potential of Table 5.

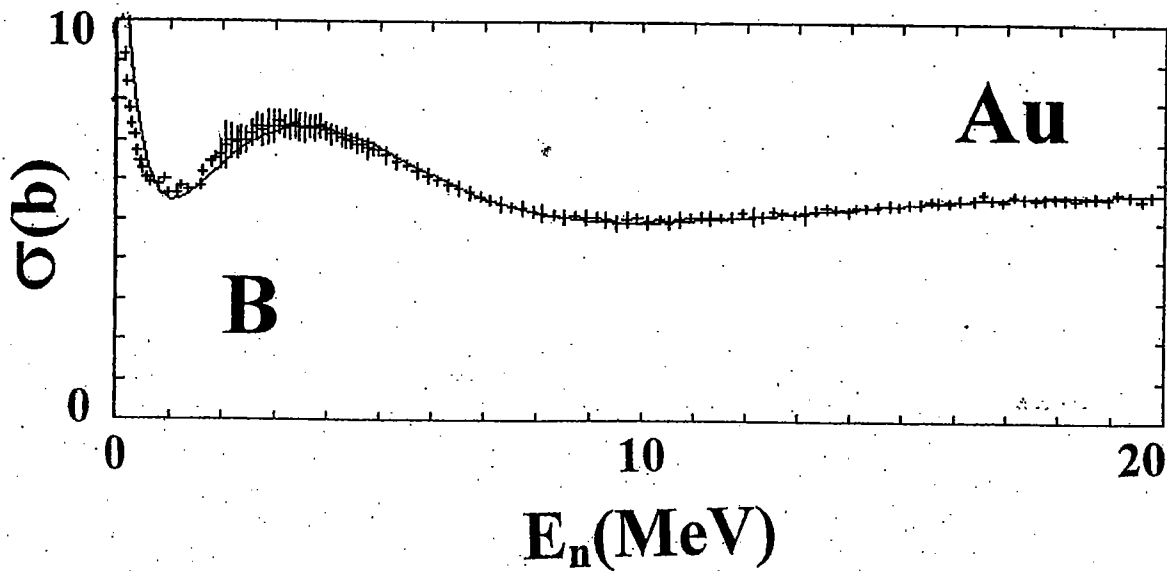
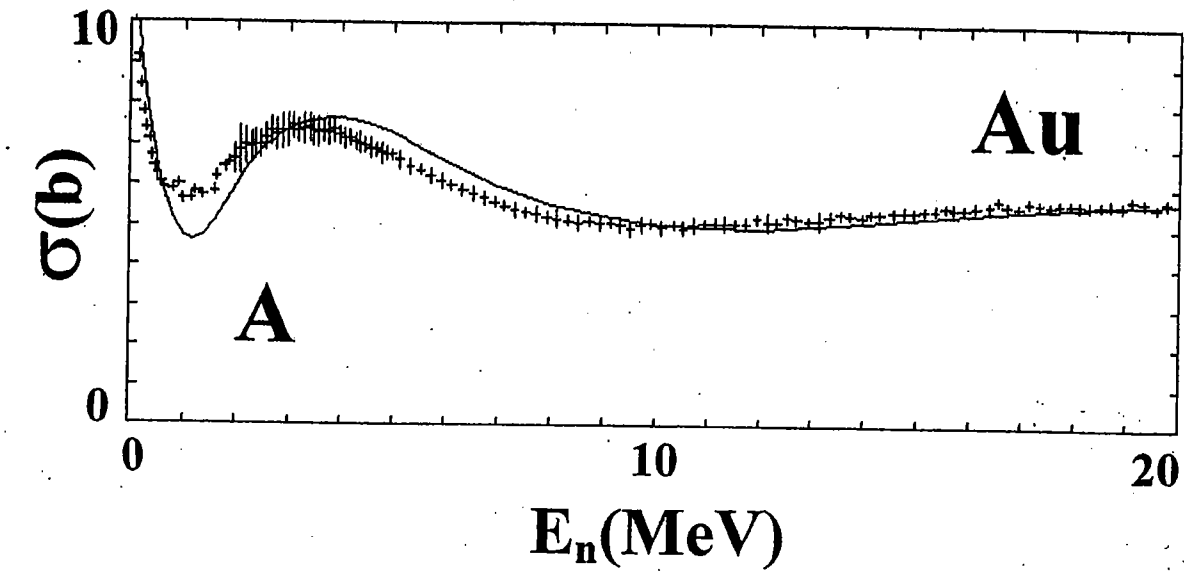


Fig. 10. Comparison of measured (symbols) and calculated (curves) neutron total cross sections of ^{197}Au . Panel A illustrates the comparisons with results calculated with the “regional” potential of Tables 6A and 6B. Panel B shows comparisons with the ^{197}Au potential of Table 3.

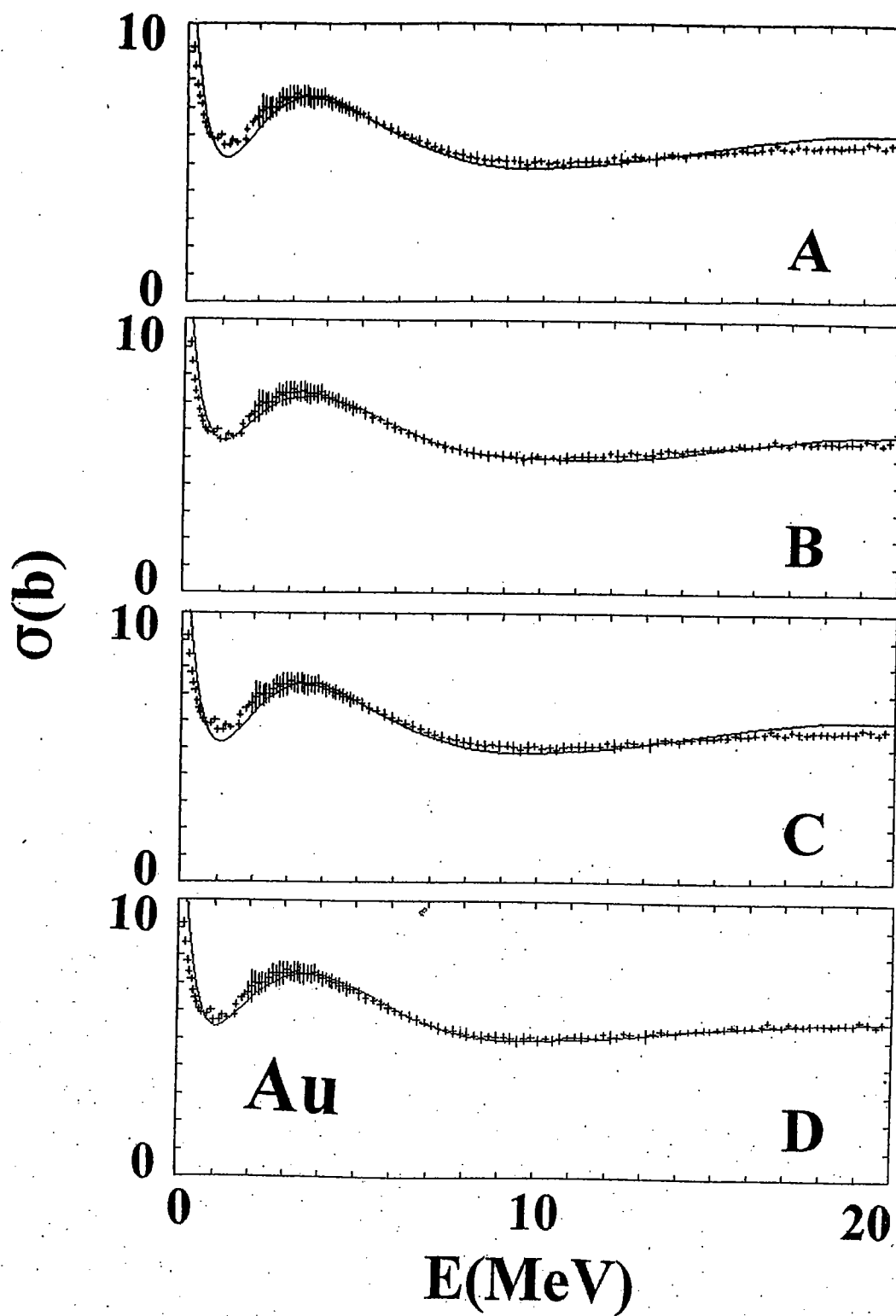


Fig. 11. Comparison of measured and calculated neutron total cross sections of ^{197}Au . The interpretation of the four panels is defined in the text.

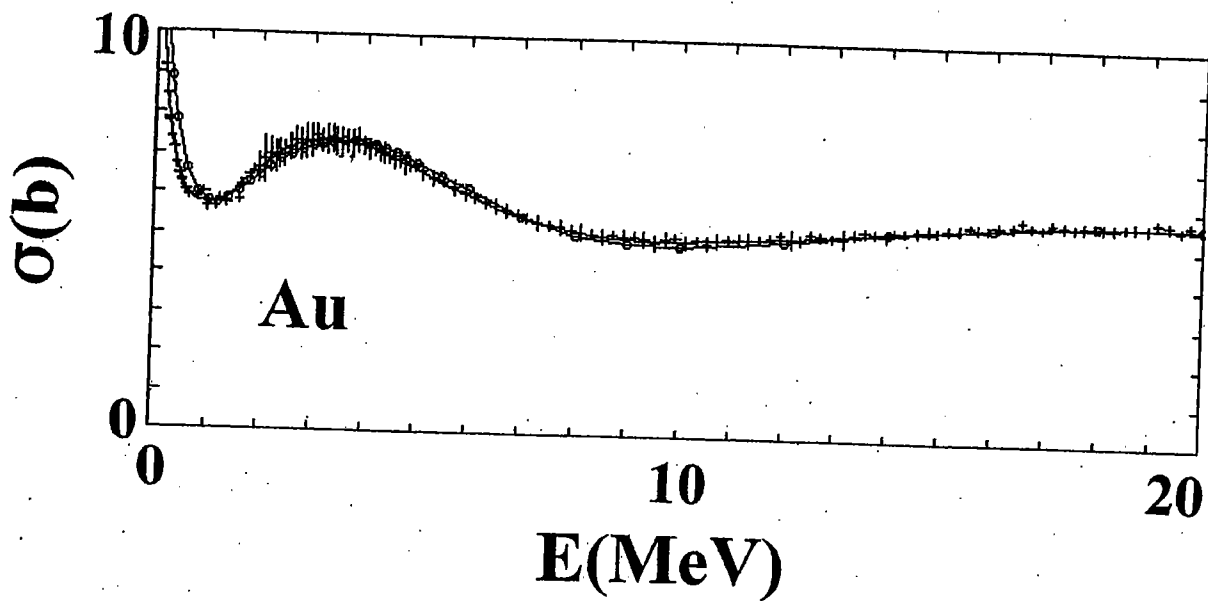


Fig. 12. ^{197}Au total neutron cross-section comparisons. The present energy-averaged experimental values are indicated with "+" symbols. The solid curve denotes the ENDF/B-VI results. The curve with additional circular symbols shows the results of the RCCM calculations using the potential of Table 3.

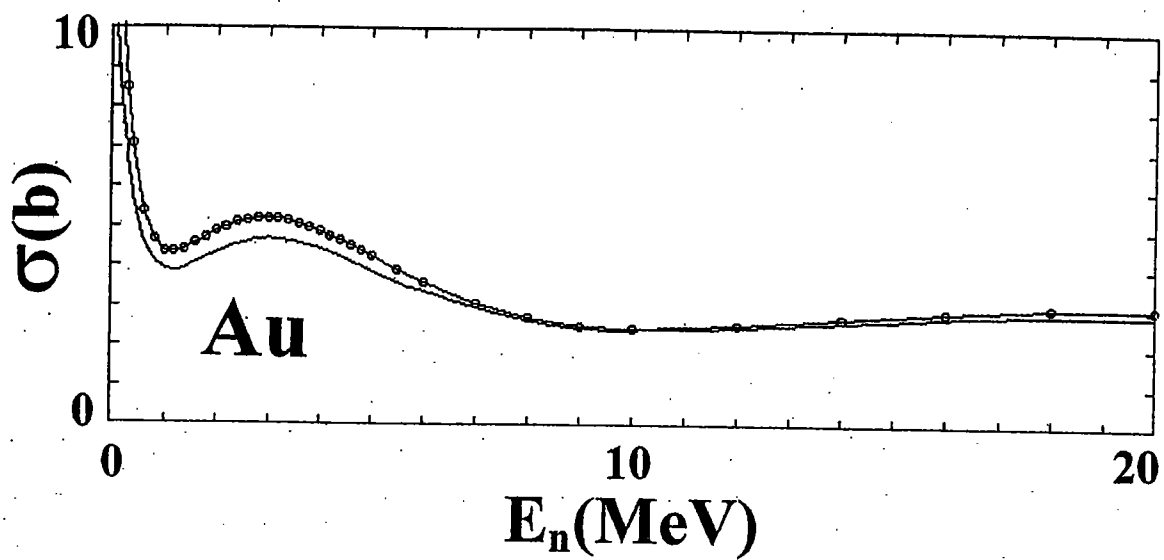


Fig. 13. Comparison of ENDF/B-VI angle-integrated elastic-scattering cross sections (simple curve) with the values calculated from the RCCM of Table 3 (curve with circular symbols).

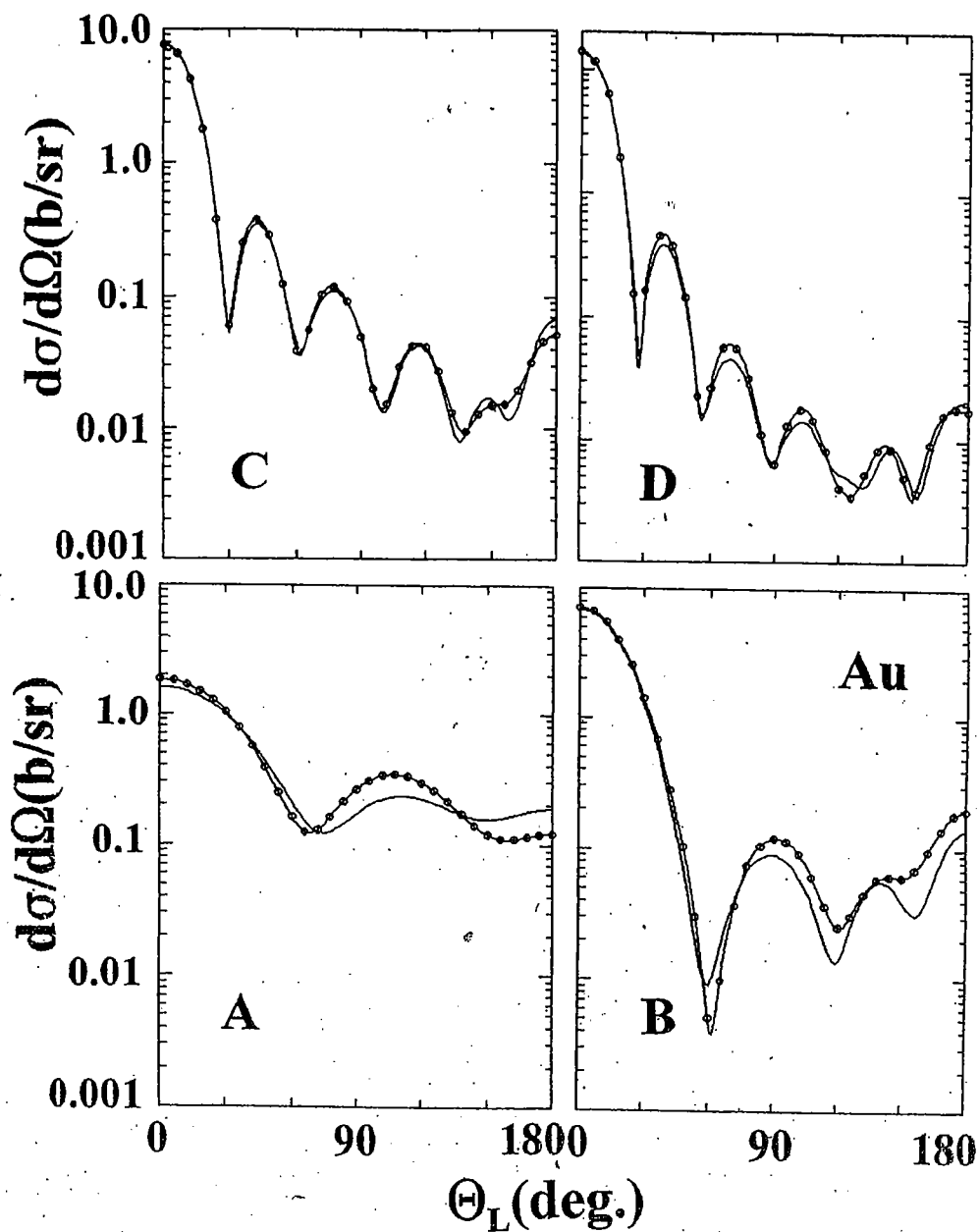


Fig. 14. Illustrative comparisons of evaluated and calculated neutron elastic-scattering differential distributions. The ENDF/B-VI distributions are indicated by simple curves. The results of calculations using the RCCM of the present work with the potential of Table 3 are indicated by the curves with circular data symbols. Panel A indicates results at 1 MeV incident energy, Panel B at 5 MeV, Panel C at 10 MeV and Panel D at 15 MeV.

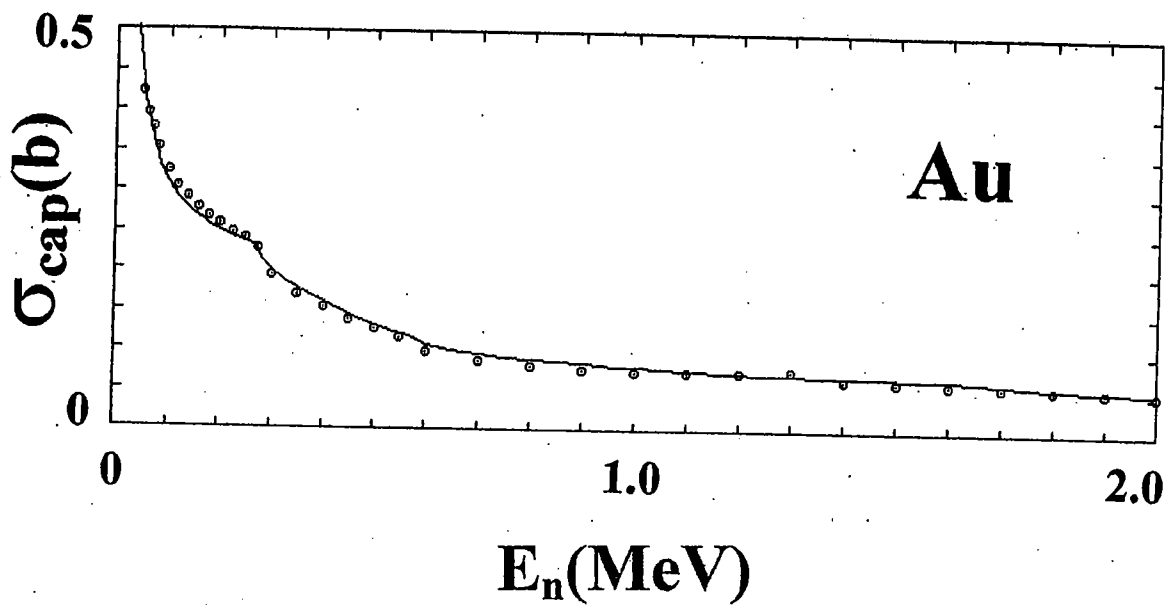


Fig. 15. Comparison of calculated and measured neutron capture cross sections of ^{197}Au . The solid curve indicates the ENDF/B-VI evaluated results, and circular symbols the results of calculations using the SOM, as described in the text.

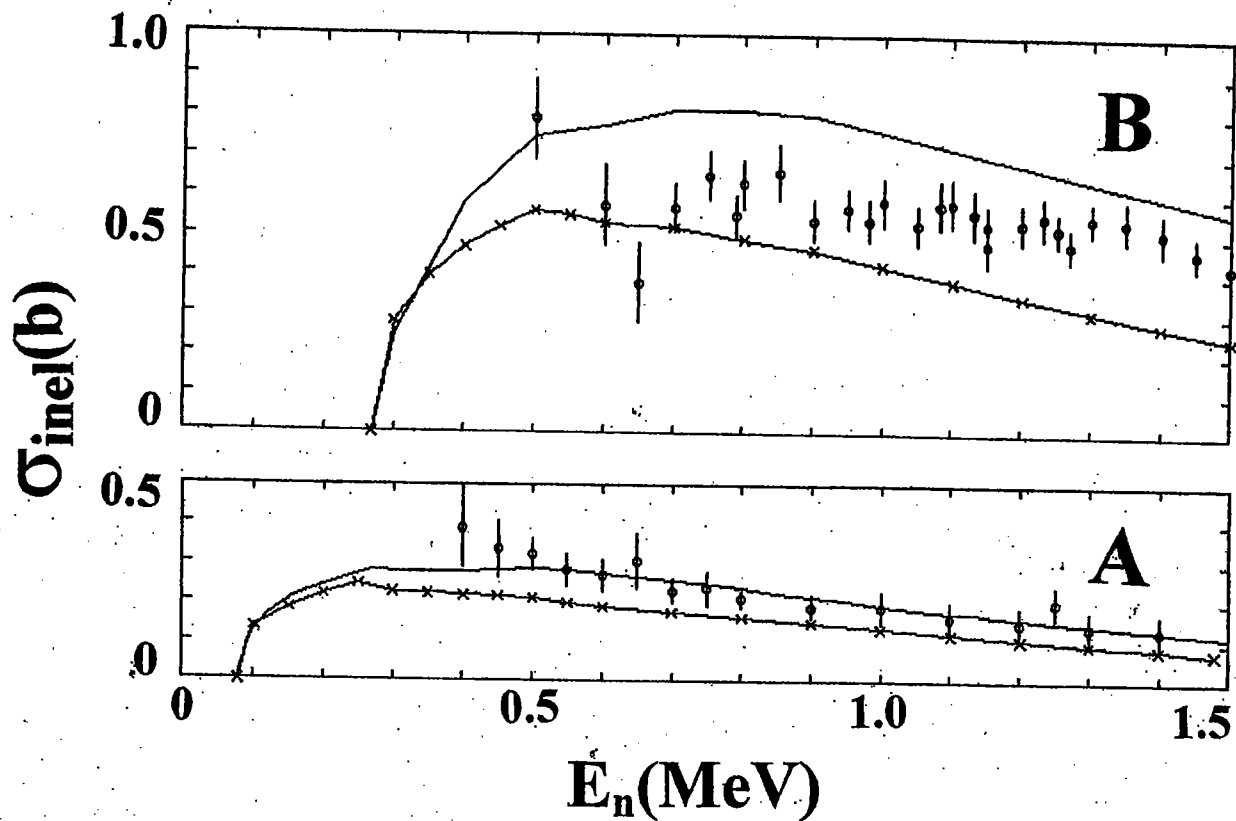


Fig. 16. Comparison of measured (circular symbols), ENDF-evaluated (simple curves) and calculated (curves with "X" symbols) inelastic excitation cross sections of ^{197}Au . Panel A pertains to the excitation of the 77 keV level and Panel B to the sum of excitations of the 269 keV and 279 keV levels, as discussed in the text.

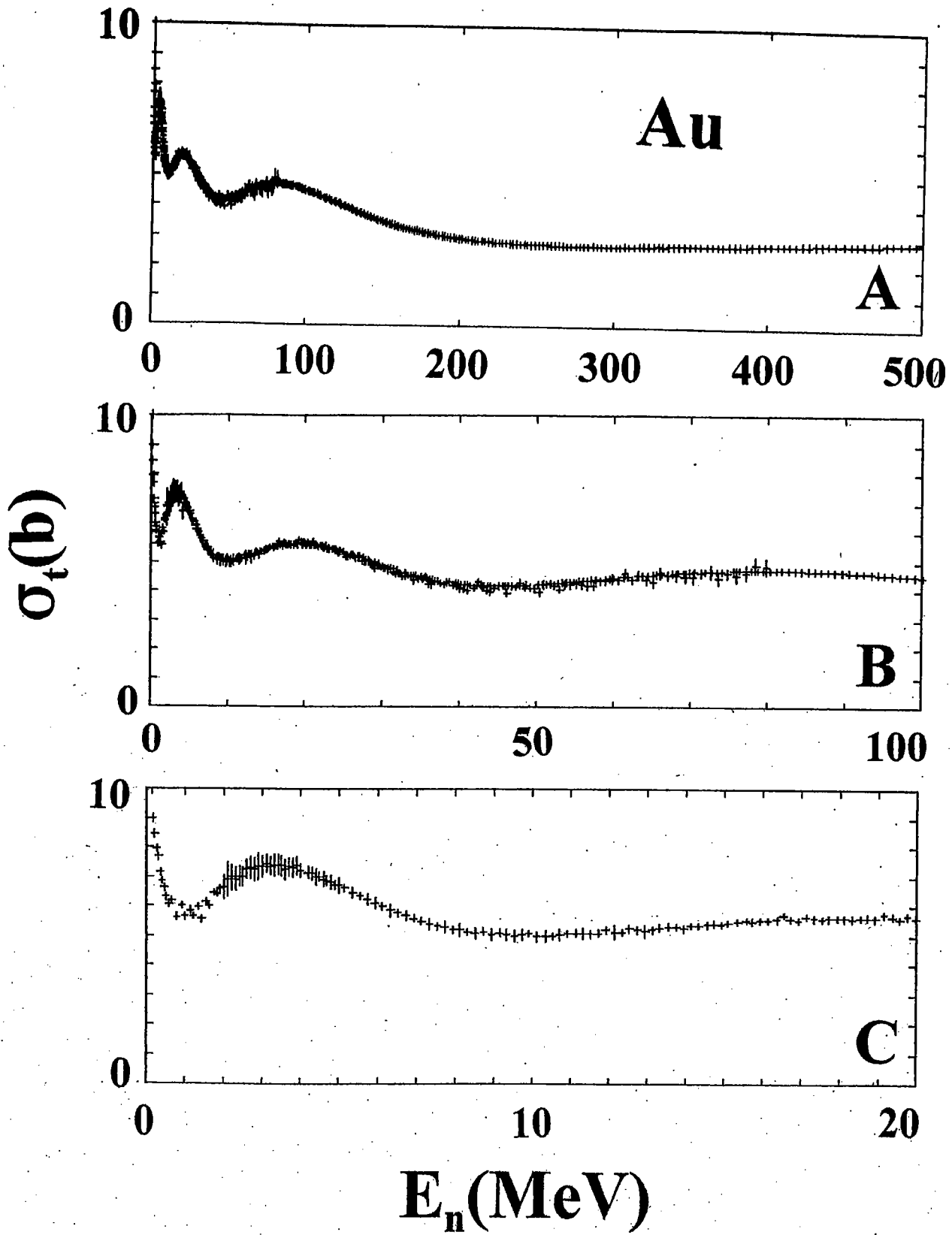


Fig. A-1. Energy ordered and averaged neutron total cross sections of ^{197}Au over the three energy ranges as numerically noted in MeV. The same experimentally based data is used in each portion of the figure, as described in the text.

